**Babeş-Bolyai University of Cluj-Napoca**

**Faculty of Chemistry and Chemical Engineering**

**Department of Physical Chemistry**

# PREPARATION AND PHYSICOCHEMICAL PROPERTIES OF SOME NANOSTRUCTURED COMPOSITES FORMAED FROM COLLAGEN, CHITOSAN AND DIVERSE BIOACTIVE INORGANIC POWDERS

**Ph.D. Thesis**

**SUMMARY**

**Scientific advisor:**

**Univ. Prof. Ph.D. Maria Tomoaia-Cotişel**

**Author:**

**Lăcrimioara-Bianca Pop**

**Cluj-Napoca**

**2011**

# TABLE OF CONTENTS

## INTRODUCTION

## *PART I*

### *CHAPTER 1*



### *CHAPTER 2*

# *PART II*

## ***ORIGINAL CONTRIBUTIONS***

## *CHAPTER 3*

## BIOACTIVE INORGANIC POWDER (BIP)

*CHAPTER 4*

# PREPARATION OF NANOSTRUCTURED COMPOSITES

*CHAPTER 5*

# IN VITRO TESTING OF BIOMATERIALS BIOCOMPATIBILITY

*CHAPTER 6*



*CHAPTER 7*



*CHAPTER 8*

*DISSEMINATION OF SCIENTIFIC RESULTS*

# INTRODUCTION

Progress of today's medical science and technology has changed significantly the medical options in solving the implants problems [1]. Biocomposites are defined as natural or man-made materials that are used directly to supplement or replace the functions of tissues of the body. Two important criteria to be fulfilled for a biomaterial is biocompatibility and biofunctionality. According to a report published in 1995 by the London Institute of Materials, it is estimated that for the global market of biocomposites about $12 billion per year are allocated [2].

Bone is composed of 69% calcium phosphate (mainly hydroxyapatite), collagen 21%, 9% water and 1% other components. There are more researches done for bone substitute composite material mainly composed of hydroxyapatite and natural or synthetic polymer. Hydroxyapatite has some good properties such as bioactivity, biocompatibility, osteoconductivity and nontoxicity but its hardness is too low. Chitosan is a natural polymer with excellent properties such as biocompatibility and bioresorbability. It is nontoxic and easily soluble in weak organic acids. Collagen, the most abundant protein from the body, is extensively studied for its biomedical applications. It is a biocompatible, biodegradable and osteoinductive material [3,4]. The extent to reconstructive orthopedic surgery it involves the development of materials in that the most important features are:

- biocompatibility with natural human bone;
- osteointegration as quickly and without side effects (necrosis, swellings);
- to act after implantation as a matrix for growth and tissue differentiation;
- to be reabsorbed by the processes of biodegradation and bone remodeling.

These materials must correspond with the structure and composition of natural bone. Materials that have best fit of these requirements are composed from calcium phosphates, namely hydroxyapatite.

This thesis had as main objectives the development of innovative technologies to achieve such biocomposites. The research to improve the functional characteristics that must meet these materials have been focused in two directions:

A. Improving the material composition with elements that are found in natural bone: silicon, magnesium and zinc. They have positive role in the development and proliferation of bone cells and provide a porous morphology and structure for the growth of the bone cells (osteoblasts).
B. Getting the nano-scale bioactive inorganic powder.

***The main working parameters in the precipitation study were****: - concentration of the solutions of reactants, temperature during the precipitation of reactants, aging time and temperature of the precipitate drying in supercritical conditions (lyophilization).*

Sorts with partially substituted HAP with varying the amounts in ions such as $SiO_4^{4-}$ (1% - 10%), $Mg^{2+}$, $Zn^{2+}$, $CO_3^{2-}$, and doped with $Ag^0$, $Au^0$ were tested in cultures of bone cells (osteoblasts). The $SiO_4^{4-}$ ions content of the grades of HAP has highlighted the role of the surface area and porosity on osteoblasts cultures. Behavior of cells in different sorts of HAP with partially

substituted ions $Mg^{2+}$, $Zn^{2+}$, $CO_3^{2-}$, and doped with $Ag^0$, $Au^0$ was compared with unsubstituted HAP and substituted sorts of HAP with 1%, 5% and 10% $SiO_2$.

In this research, we prepared by precipitation over 20 varieties of nano hydroxyapatite (HAP) pure HAP and partially substituted HAP with ions that are found in bone composition and HAP doped with nanoparticles of gold or silver. Physico-chemical characterization of HAP nanoparticles and their nanobiostructures with chitosan and collagen was made by FTIR spectroscopy and XPS, X-ray diffractometry, specific surface area and porosity analysis by BET and thermal analysis TG, DTG, DTA and DSC. Powder stability was demonstrated by thermogravimetric analysis; structure and morphology of the materials were characterized by SEM, TEM and AFM imaging techniques.

*The thesis is divided into eight chapters*

In ***Chapters 1 and 2*** are discussed, based on bibliographical research, the main theoretical aspects concerning the structure and composition of natural bone, inorganic nanostructures based on HAP and synthetic or natural polymers, as well as theoretical considerations regarding the formation of nanostructured inorganic phase (Chapter 2).

***Chapter 3*** contains original contributions in preparation of unsubstituted and substituted hydroxyapatite with different ions such as $SiO_4^{4-}$ (1% - 10%), $Mg^{2+}$, $Zn^{2+}$, $CO_3^{2-}$, or doped with $Ag^0$, $Au^0$, physico-chemical characterization of the synthesized materials was made by FTIR and XPS spectroscopy, X-ray diffractometry and specific surface area and porosity analysis by BET and thermal analysis TG, DTG, DTA and DSC.

***Chapter 4*** contains information about the preparation of biocomposites with HAP and natural polymers, chitosan and collagen and their physico-chemical characterization.

***Chapter 5*** presents the results of biocompatibility of nanostructures in cells culture of osteoblasts. The proliferation and cell adhesion phenomena on fibrous scaffolds in osteoblasts cells cultures are evidenced.

***Chapters 6, 7*** and ***8*** contain general conclusions, bibliography and dissemination of scientific results.


## KEYWORDS

Hydroxyapatite
Collagen
Chitosan
Composites
Osteoblast cells

# CHAPTER 3 - ORIGINAL CONTRIBUTIONS

## INORGANIC BIOACTIVE POWDER (PIB)

### 3.1 Preparation of bioactive inorganic powder

Hydroxyapatite even with high biocompatibility, can be substantially improved by modifying the chemical composition and morphological structure. These changes are favored by the ability to accept easily in its structure many substitute ions for $Ca^{2+}$ and for $PO_4^{3-}$ with the changing of chemical composition and morphological structure [223-226]. Chemical and structural analysis showed that the inorganic phase of bone does not correspond to the stoichiometric formula of hydroxyapatite. Virtually the inorganic phase in bone tissue is a mixture of inorganic compounds based on hydroxyapatite, where $Ca^{2+}$ ions and $PO_4^{3-}$ ions are partially substituted with various other ions (anions and cations). Substituent ions must be biocompatible with the body in order that their resorption does not cause unwanted reactions and the rejection phenomena. Moreover, the presence of foreign ions in hydroxyapatite structure confers an enhanced ability to stimulate the growth of bone tissue. Besides the above mentioned conditions, substituent ions should provide good biocompatibility with a series of natural polymers (chitosan, collagen) or synthetic polymers (polyacrylic acid, polymethyl metacrylate, etc..) [229].

Although the presence of substitute ions in the structure of hydroxyapatite is in small proportion, they confer specific biological and physical properties so that their role is important for determining the bone chemistry. Therefore, the presence of substituted ions in the hydroxyapatite structure is required for biocomposites in order to present the biostructure and biochemistry of the natural bone. Their presence is also important for ensuring a high rate of regeneration of the bone tissue and physicochemical parameters close to thpose of natural bone The most important substitute ions for hydroxyapatite in biomedical materials applications are $Mg^{2+}$ and $Zn^{2+}$ for $Ca^{2+}$ ions and $CO_3^{2-}$ and $SiO_4^{4-}$ for $PO_4^{3-}$ ions. $Mg^{2+}$ ions play an important roleby the nature of transformations induced by them in bone matrix. Lack of magnesium in the bone, adversely affects physiological processes in bone metabolism, leading to increased the fragility of bones [234-236].

Synthetic hydroxyapatite substituted with magnesium hydroxyapatite is more soluble than pure hydroxyapatite, and this makes its resorption in body much faster, thus accelerating the regeneration process of natural bone. Nevertheless, there is a limiting ration for the Mg content, since a $Mg^{2+}$/ $Ca^{2+}$ mole ratio over 0.3 determines the formation of tricalcium phosphate and magnesium phosphate $Mg_3(PO_4)_2$ instead of magnesium-hydroxyapatite (MgHAP). Along with magnesium, another essential element with stimulating effect on bone formation is *zinc*, which is found in bone as much as 0.012% - 0.0225 %. The presence of zinc, on the other hand, contributes to an increased bone protein (collagen) content, because it enhances the alkaline phosphatase activity and inhibits the resorption process of amorphous hydroxyapatite, thus

avoiding local inflammations in bones [234]. Moreover, the presence of $Zn^{2+}$ ions in the solution during the precipitation, inhibits the growth of HAP particles, facilitating the obtaining of nano-scale biocomposites [236].

*Silicon* present in hydroxyapatite structure as $SiO_4^{4-}$ ions plays an essential role in biological processes, determining the chemical structure of bone. Substitution of $PO_4^{3-}$ ions in hydroxyapatite with $SiO_4^{4-}$ ions increases the osteoblastic cells activity in comparison with pure hydroxyapatite. This increase in the activity of osteoblasts leads to faster bone remodeling, thus reducing its regeneration time. The presence of silicon in hydroxyapatite structure increases other biological phenomena as well, such as cell adhesion and a more rapid development of organic matrix (collagen) in bone structure [225]. Although there are several methods of synthesis for hydroxyapatite, no product was yet manufactured, to comply in a satisfactory manner with all quality conditions necessary for the biocomposites used in implants and bone reconstruction*: nanoscale particles, high crystallinity, good biocompatibility with natural bone tissue, and high resorption rate.* Existing manufacturing processes do not eliminate the appearance of secondary phases, made of α- and β-tricalcium phosphate $Ca_3(PO_4)_2$, and of silicocarnotite ($Ca_{10}(PO_4)_4(SiO_4)_2$), phases, negatively affectig biological properties [228, 231].

The degree of crystallinity to be achieved in hydroxyapatite structure is is attained in practice by calcination at temperatures between 600°C and 1300°C, but in these conditions a sintering of the material takes place, leading to an increas in particles size, even though they were initially obtained at the nano scale. During the heat treatments applied, because the phenomenon of sintering, the particles grow from nano to microscale. It is known that nano-scale particles and their high crystallinity influence positively the growth and the development of bone cells (osteoblasts), by means of which natural bone tissue is regenerated.

*Our original research aimed to prepare bioceramics based on HAP with good biocompatibility and bioactivity, with high resorption rate and without any side effects.* Sveral researchers evidenced the positive effects of substituent ions, such as $Mg^{2+}$, $Zn^{2+}$, $CO_3^{2-}$ şi $SiO_4^{4-}$, in the structure of ceramics. However, in literature no compositions of ceramics based on HAP with complex structure are reported, containing all these ions simultaneously in the HAP structure.

*The main routes of hydroxyapatite synthesis are sol-gel, airgel, solid phase reaction, precipitation and hydrothermal method* [19]. Among these, precipitation seems to present the best perspectives, because it uses cheap reagents, easily accessible: a soluble calcium salt (nitrate or acetate) $Ca(NO_3)_2 \cdot H_2O$ or $Ca(CH_3COO)_2 \cdot yH_2O$; a soluble phosphate: sodium or potassium phospahte, but preferably $(NH_4)_2$ $HPO_4$, and ammonia solution to correct the pH in the desired range. Preparation by precipitation method requires simple installations, a technological flow easy to control, thus allowing to obtain materials with superior and easily reproducible properties. For the synthesis of hydroxyapatite we used an original installation shown in Figure 3.1. The raw materials used are listed in Table 3.1

Figure 3.1 Installation fir hydroxyapatite preparation.

Table 3.1 Raw materials used in preparing hydroxyapatite powders and biocomposites:

| Chemical compound | Chemical formula | The manufacturer |
|---|---|---|
| Calcium nitrate | $Ca(NO_3)_2 \cdot 4H_2O$ | Merck Germany |
| Diamonium hydrogen phosphate | $(NH_4)_2 HPO_4$ | |
| Ammonia | $NH_3$ | |
| Nonylphenol | $C_{15}H_{24}O$ | |
| Glacial acetic acid | $CH_3COOH$ | |
| Magnesium nitrate | $Mg(NO_3)_2 \cdot 6H_2O$ | |
| Tetraethyl ortosilicate (TEOS ) | $SiC_8H_{20}O$ | |
| Absolute ethyl alcohol | $CH_3\text{-}CH_2OH$ | |
| Zinc nitrate | $Zn(NO_3)_2$ | |
| Silver nitrate | $AgNO_3$ | |
| Chloroauric acid 99.5% | $HAuCl_4 \cdot 4H_2O$ | |
| Collagen type I (bovine-Achilles tendon) | | Sigma- Aldrich USA |
| Chitosan (medium molecular weight) | | |
| Glutaraldehyde (GA) 25% in $H_2O$ | $CH_2(CH_2CHO)_2$ | |
| Sodium silicate | $Na_2SiO_3$ | Prepared in the laboratory |

### 3.1.1 Hydroxyapatite

HAP preparation was made by precipitation method with a sequence of operations that are illustrated in Figure 3.3.

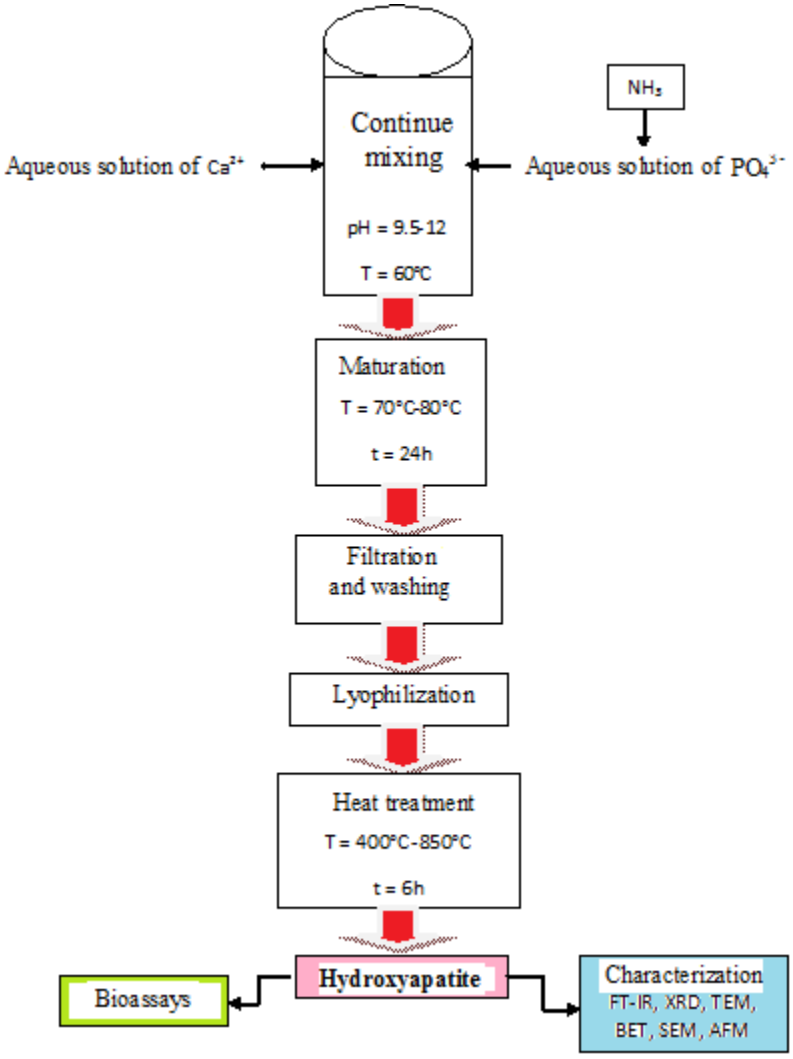


Figure 3.3 Scheme of hydroxyapatite preparation by precipitation method.

As a source of calcium ions we used 0.15M $Ca(NO)_3 \cdot 4H_2O$ solution and as a source of phosphate ions we used 0.09M $(NH_4)_2HPO_4$ solution. Crystallite growth was prevented by the addition of nonylphenol as surfactant in both solutions, of calcium and phosphate ions. The precipitation reaction was executed under intense stirring at a temperature of 60°C, by fast

adding (2-3 seconds) the solution with calcium ions and then the phosphate solution. After precipitation, the reaction mass was subjected to hydrothermal treatment for 24 hours at 70°C for the maturation of the precipitate. Resulting suspension was filtered and the precipitate was washed with ultrapure water. The precipitate obtained was dried by lyophilization, thus avoiding the coalescence of crystallites. Prepared powder was subjected to thermal treatment within 400-850°C over 6 hours and then physico-chemically characterized.

### 3.1.2 Hydroxyapatite modified with silica

Silicon is one of the essential elements present in biological processes. Its importance in bone formation has been scientifically proven. Substitution of phosphate ions by silicate ions in the structure of hydroxyapatite increased bone cell activity as compared with physiological hydroxyapatite. The result is a rapid remodeling of its surface, which has been observed in substituted hydroxyapatite with silicate ions (Si-HAP). The percentage of silica present in the biological hydroxyapatite is within the range from 0.2 wt % and 0.8 wt %. The presence of silicon in HAP favors the cellular adhesion and development of organic phase of bone, collagen.

Molar percentage of silicate ions in hydroxyapatite should to be between 0.1 % and 2,5 %. The literature indicates that an important property of biocomposites along with crystallinity, is porosity and specific surface area [225]. Hydroxyapatite with controlled porosity and specific surface area can be obtained by inserting in its structure $SiO_4^{4-}$ ions under various forms such as TEOS or $Na_2SiO_3$. These ions by a polycondensation process create siloxane groups Si-O-Si- and silanol groups Si-OH (Figure 3.4), depending on the HAP:$SiO_2$ ratio, temperature, hydrodynamic conditions and rate of adding reactive components.

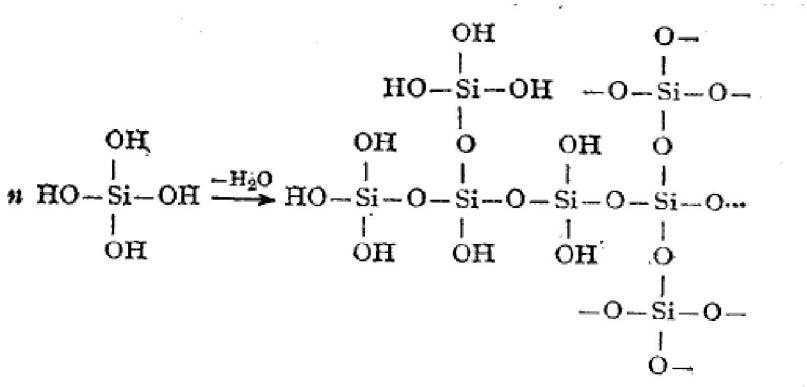


Figure 3.4 Macromolecular and three-dimensional structures of hydrated $SiO_2$.

To this end, in the syntheses that will be presented, the parameter that was changed in the HAP structure was the final concentration of silicon dioxide. In addition to the polycondensation, $SiO_2$ creates a porous structure, and its adsorption on the surface of calcium phosphate particles prevents the growth of crystallites and has also an inhibitory role [225, 226]. Another important

parameter in the crystallization process is temperature, which influences both the nucleation process and the growth of nuclei.

In order to control the final size of particels, in all our syntheses the precipatation process occured at 60°C. At this temperature there is a significant increase of the transformation rate of β-witchlonite (the compound formed in the first step of precipitation) to the hydroxyapatite structure. In order to prevent particles agglomeration and growth, the surfactant nonyl phenol was added, whose adsorption on the particels surface limits their growth.

Nanohydroxyapatite powder substituted with 1 wt %, 5 wt % and 10 wt % silica ($SiO_2$) was prepared by precipitation method in a similar way as the synthesis of pure hydroxyapatite except that $SiO_2$ was added as a 5 wt % sodium silicate solution ( $Na_2O$: $SiO_2$ = 1:3.2) in the diammonium phosphate solution. In Figure 3.5 we present the functionalization of HAP nanoparticles with $SiO_2$.

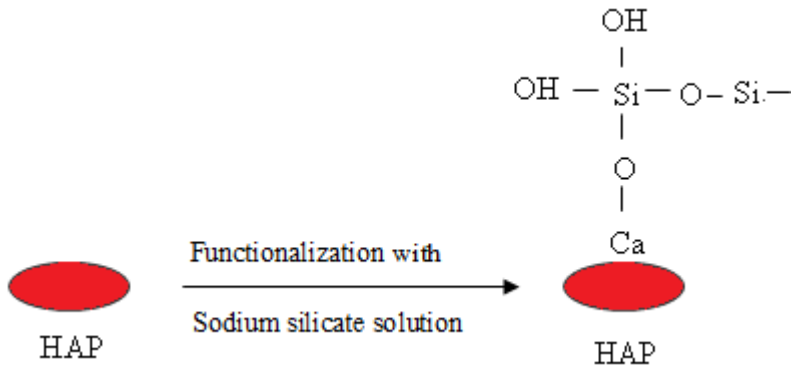


Figure 3.5 Functionalization of HAP nanoparticles with $SiO_2$.

### 3.1.3 Hydroxyapatite modified with magnesium

The presence of substituent ions in the structure of hydroxyapatite is essential for the biocomposites in order to have a biostructure and biochemistry similar to those of natural bone. On the other hand, they assure a higher regeneration rate of bone tissue. The most bimportant substituent ions are $Mg^{2+}$, $Zn^{2+}$, $CO_3^{2-}$ and $SiO_4^{4-}$ [247]. To this aim, we prepared different sorts of hydroxyapatite with complex structure, substituted with magnesium, silicon and zinc, presented in Table 3.3. This magnesium substituted hydroxyapatite was prepared similarly tp pure hydroxyapatite, but $Mg^{2+}$ ions were introduced in the solution with $Ca^{2+}$ ions.

### 3.1.4 Hydroxyapatite modified with magnesium and silicon

These complex samples were prepared similarly to pure hydroxyapatite, but $Mg^{2+}$ were introduced in the solution with $Ca^{2+}$ ions, and $SiO_4^{4-}$ was introduced as TEOS in the solution with phosphate ions, after brnging its pH value in the range 11.5-12 with a 25% ammonia solution, before mixing the two solutions. In order to prevent a precipitation of $SiO_2$ when TEOS is added,

this component was previously diluted in a 5% ethyl alcohol solution, and then the solution was diluted to 0.5 % with ultrapure water. The concentration of substituents in HAP was 0.2%$SiO_2$, 0.6%Mg, and 0.2%Zn

Table 3.3 Chemical composition of complex hydroxyapatite samples

| No. | Bmposition of complex hydroxyapatite (%) | Calcination temperature °C |
|---|---|---|
| 1 | HAP_0.2%Mg | 450, 650, 850 |
| 2 | HAP_1%$SiO_2$ | 450, 650, 850 |
| 3 | HAP_0.4%$SiO_2$_0.2%Mg | 450, 650, 850 |
| 4 | HAP_0.2%$SiO_2$_1.5%Mg | 450, 650, 850 |
| 5 | HAP_1%$SiO_2$_1.5%Mg | 450, 650, 850 |
| 6 | HAP_0.2%$SiO_2$_0.6%Mg_0.2%Zn | 450, 650, 850 |
| 7 | HAP_0.2%Mg_0.6%Si_0.2%Zn + 0.14% Ag | 450, 650, 850 |
| 8 | HAP_0.2%Mg_0.6%Si_0.2%Zn+0.3% Au | 450, 650, 850 |

### 3.1.5 Hydroxyapatite modified with magnesium, silicon and zinc

The preparation of these samples with complex structure was performed similarly as the synthesis of pure hydroxyapatite, except that $Mg^{2+}$ ions with $Zn^{2+}$ ions are introduced into the solution with $Ca^{2+}$ ions., and $SiO_4^{4-}$ ions are introduced as TEOS in the solution with phosphate ions after adjusting its pH at 11.5-12 with 25 wt % ammonia solution, a few minutes before the two solutions are mixed. To avoid the precipitation of $SiO_2$ when added as TEOS, this substance is previously diluted in 5 % ethylic alcohol solution, and then the solution is diluted to 0.5 % with ultrapure water. The concentration of substitutents in the structure of HAP was 0.2 wt % $SiO_2$, 0.6 wt % Mg and 0.2 wt % Zn.

### 3.1.6 Complex hydroxyapatite doped with silver nanoparticles

#### Silver - role and biological effects

One of the most remarkable aspects of colloidal silver is that it has an extremely wide range of biomedical applications and uses. While a conventional pharmaceutical antibiotic is effective against six or seven types of germs and totally inefficient against viruses, often leading to unwanted side effects, silver is lethal for more than 650 types of bacteria, viruses and fungi, without being toxic for the human body. Unlike synthetic drugs that chemically react with certain enzymes, biological action of silver is of catalytic type. Its presence is suffocating viruses, bacteria and fungi without any harm to multicellular organisms, which have a totally different enzyme system. Laboratory tests have shown that colloidal silver (5-10 ppm) kills most

of bacterias, fungi and viruses in 2-6 minutes of contact. Particles generating colloids are in the range of size from 0.001 µm to 0.1 µm.

The action of silver ions is not limited to bacteria, drugs containing silver can destroy hundreds of viruses, fungi, and protozoa. Lately nano silver ions showed the ability to fight with cancer. Thus, it was shown that colloidal silver solutions are able to inhibit the mobility and tumor cell adhesion [204-210]. It was found that these particles with sizes between 2 and 10 nm are able to adsorb and destroy bacteria which affect human tissues *in situ* and improve immune mechanisms and the tissue repair [211-216]. Scientific experiments have shown that colloidal silver is effective in treating many diseases: microbial infections, fungal, parasitic and viral infections of the skin, sensory organs, the digestive tracts, respiratory and urinary autoimmune diseases and even cancer. The reconstruction healing of tissues is accelerated in the presence of silver. Scars develop when the undifferentiated cells does not exist in sufficient numbers. Based on this, there is evidence that colloidal silver would reduce or eliminate internal scars and speed healing after surgical operations. Good results were obtained in faster recovery after fractures, muscle tears or ligament, sprain, sprains, burns, skin ulcers, etc.

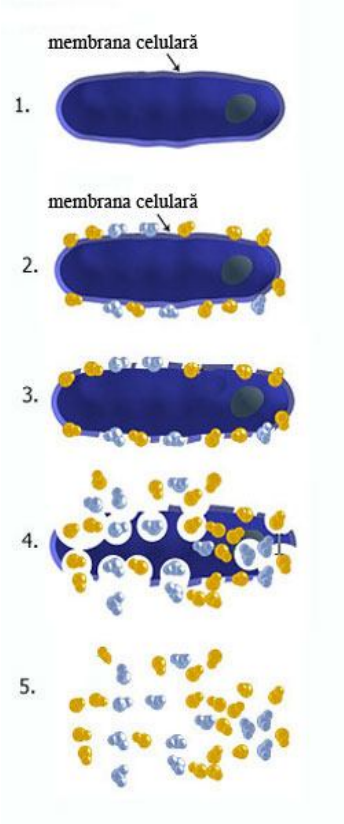


Figure 3.6 The action of silver mechanism

Biofuctionality and catalytic action of silver is attributed to the fact that it has the ability to adsorb at the surface of proteins that are involved in biological processes, and thus increasing their reactivity (Fig. 3.6).

### 3.1.6.2 Preparation of complex hydroxyapatite doped with silver nanoparticles

Preparation of this material was similar to the synthesis of complex hydroxyapatite (with magnesium, silicon, zinc). The suspension of complex HAP obtained is filtered, washed, and the precipitate is redispersed in an aqueous solution to obtain a very dilute suspension of complex HAP. In the suspension a silver nitrate solution is added (0.001 M concentration). To this final suspension sodium borohydride is added, in order to reduce silver in the system. The final suspension aging accurs on a water bath at a temperature of 70°C for 24 hours. After aging, the suspension is filtered, washed and lyophilized. The powder obtained is calcinated at a temperature of 650°C for 6 hours, and then grinded in an aluminum ball mill for 4 hours to

obtain a homogeneous nanometric sized powder. We obtained a white powder with the chemical composition **HAP_0.2%Mg_0.6%Si_0.2%Zn + 0.14% Ag.**

### 3.1.7 Complex hydroxyapatite doped with gold nanoparticles

#### 3.1.7.2 Preparation of complex hydroxyapatite doped with gold nanoparticles

Preparation of this material wascarried out similarly to the synthesis of hydroxyapatite with complex structure (magnesium, silicon, zinc). Hydroxyapatite suspension obtained is filtered, washed, and the precipitate is redispersed in an aqueous solution so that we get a very dilute suspension of complex HAP. To this suspension an 1% solution of tetrachloroauric acid trihydrate is added, previously diluted in aqueous solution so that the final concentration is $10^{-3}$ M. To this suspension, sodium borohydride is added in order to reduce the gold in the system. The aging of the final suspension (HAP + Au) was done on the water bath at the temperature of 70°C for 24 h. After aging, the suspension is filtered, washed and lyophilized. The powder obtained is calcinated at a temperature of 650 ° C for 6 hours and than grinded in an aluminum ball mill for 4 hours, to obtain a homogeneous nanometric sized powder. We obtained a pink powder with composition **(HAP_0.2%Mg_0.6%Si_0.2%Zn + 0.3% Au).** A scheme for the preparation of hydroxyapatite with gold nanoparticles is shown in Figure 3.7.

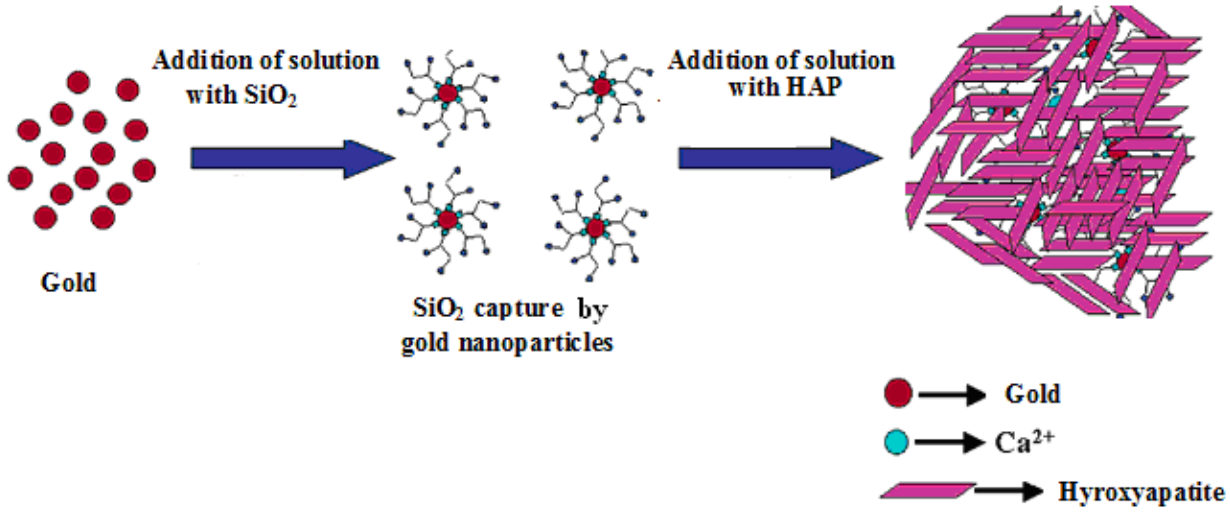


Figure 3.7 Scheme for the preparation of hydroxyapatite doped with gold nanoparticles.

## 3.2 CHARACTERIZATION AND PHYSICOCHEMICAL PROPERTIES OF BIOACTIVE INORGANIC POWDERS

In order to correlate biological activity in osteoblasts cell cultures with physico-chemical structure of the mineral phases, we made a characterization involving measurements of porosity (BET), X-ray diffractometry, FTIR, XPS, SEM, TEM, AFM and TG, DTA, DSC.

### 3.2.1 XPS spectroscopy

This method, also known as Electron Spectroscopy for Chemical Analysis (ESCA) is used to analyze the chemical composition of surfaces and allows for the identification all chemical elements, except for H and He (atoms without inner electron shells). Survey spectra were performed (e.g. Fig. 3.9) for samples HAP_MgSiZn; HAP_MgSiZn+Ag; HAP_MgSiZn+Au; HAP_MgSiZn+CHI/$SiO_2$+COL/$SiO_2$. Based on survey spectra, table 3.4 includes the relative concentration of main elements in the samples studied.

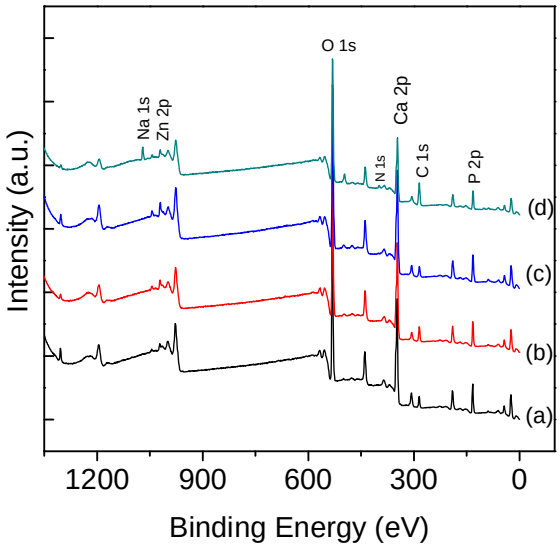


Figure 3.9 XPS survey spectra of samples: (a) HAP_MgSiZn (b) HAP_MgSiZn + Ag, (c) HAP_MgSiZn + Au, (d) HAP_MgSiZn + CHI/SiO2 + COL/SiO2.

.

Table 3.4 Relative concentration of the main elements determined from survey spectra.

| Hydroxyapatite sample | Elemental composition (at %) | | | | | | | | | | |
|---|---|---|---|---|---|---|---|---|---|---|---|
| | **Ca** | **O** | **C** | **P** | **Mg** | **Zn** | **N** | **Na** | **Si** | **Ag** | **Au** |
| HAP_0.67%Mg_0.28%Si_ 0.2%Zn | 23.2 | 53.7 | 1.1 | 21.2 | 0.6 | 0.2 | - | - | - | - | - |
| HAP_0.67%Mg_0.28%Si_ 0.2%Zn+0.14%Ag | 23.1 | 55.2 | 1.2 | 20.1 | 0.2 | 0.1 | - | - | - | 0.1 | - |
| HAP_0.67%Mg_0.28%Si_ 0.2%Zn+0.3%Au | 23.6 | 54.3 | 1.1 | 20.1 | 0.4 | 0.2 | - | - | - | - | 0.3 |
| HAP_0.67%Mg_0.28%Si_ 0.2%Zn+CHI/$SiO_2$+COL/$SiO_2$ | 15.9 | 41.4 | 24.1 | 13.3 | 0.5 | 0.1 | 1.5 | 1.7 | 1.5 | - | - |

Survey spectra have photopeaks corresponding to elements that are included in the composition of systems. Thus photopeaks that correspond to Ca 2p, O 1s, P 2p, C 1s, Zn 2p were identified for all samples investigated, excepting the photopeaks for N 1s and Na 1s from sample (d) HAP_MgSiZn+CHI/$SiO_2$+COL/$SiO_2$, due to the presence of collagen and chitosan in the sample structure. The photopeak of Na 1s is due to collagen and chitosan functionalization with sodium silicate. From the table it can be seen that for sample functionalised with COL, the detection of the basic elements of the samples was less obvious because of the protein layer formed on the surface of HAP particles. The photopeak for C 1s is higher in the sample with CHI and COL du to their presence in the system. The photopeak N 1s is situated around 400 eV and is typical for nitrogen from organic matrices.

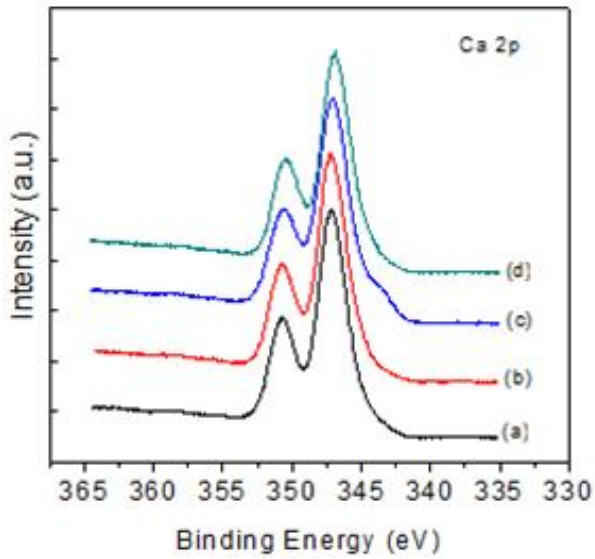


a

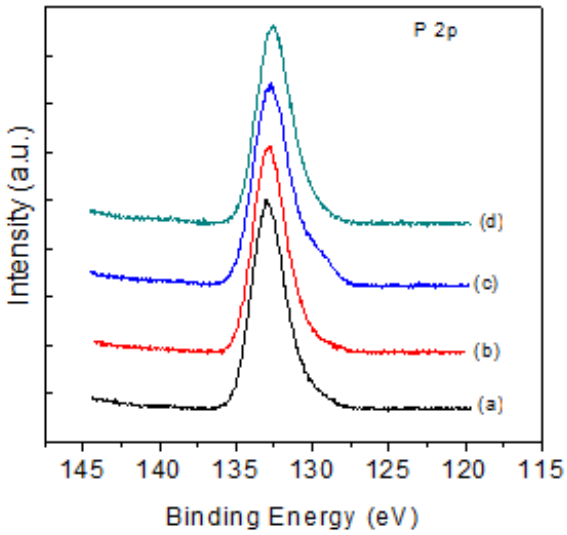


B

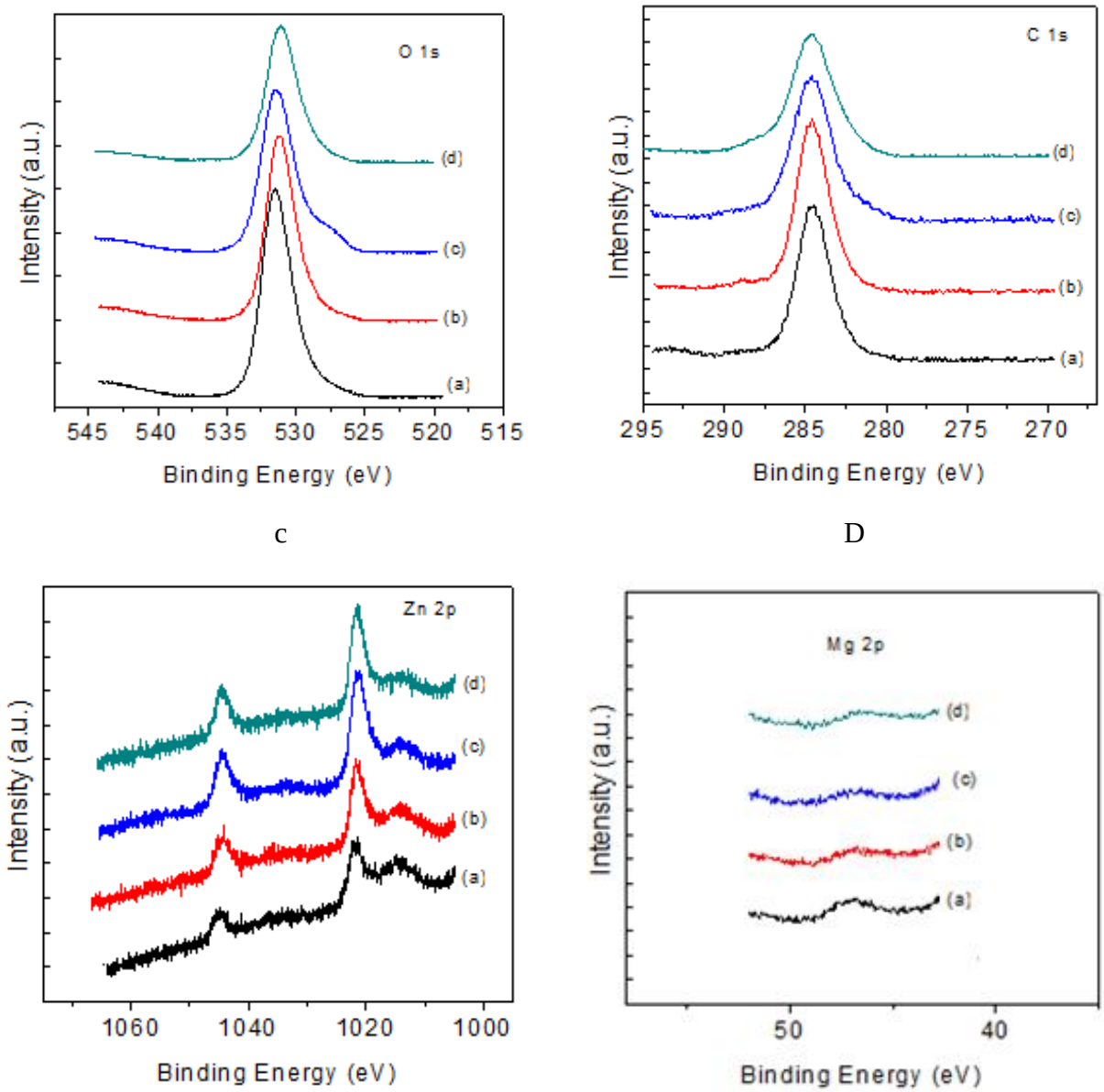


Figure 3.10 High resolution spectra for photopeaks of: (a) Ca 2p, (b) P 2p, (c) O 1s, (d) C 1s, (e) Zn 2p, (f) Mg 2p.

From high-resolution XPS spectra (Fig. 3.10) we can observe a slight shift of the signal given by photoelectrons O 1s, from about 531.6 eV energy (sample HAP_MgSiZn) to 531.1 eV (sample HAP_MgSiZn+0.14 wt % Ag), respectively 531.2 eV (samples HAP_MgSiZn + 0.3 wt % Au and HAP_MgSiZn+CHI/$SiO_2$+COL/$SiO_2$) (Figure 3.10 c). The decrease of electron energy shows a higher electron density on oxygen atoms tham on the cations bonded to it in structural units. High-resolution spectra (Fig. 3.10 a, b and c) for the photopeaks of Ca 2p, P 2p

and O 1s show a slight shift of the signal in the sample containing gold (HAP_MgSiZn + 0.3 wt % Au). This shift is due to the high electron density at the surface of gold nanoparticles, which determines by inductive effect interactions with $Ca^{2+}$, $P^{5+}$ and $O^{2-}$ from the structure of hydroxyapatite.

### 3.2.2 FTIR spectroscopy

We used FTIR spectroscopy to determine the characteristic peaks of hydroxyapatite and interactions that occur between the compounds existing in its structure [233]. Figure 3.11 a-h presents the FTIR spectra of HAP samples before and after heat treatment at 650C °, HAP with 1%, 5%, 10% $SiO_2$, HAP_MgSiZn, HAP_MgSiZn+Au and HAP_MgSiZn+Ag after heat treatment at 650 °.C

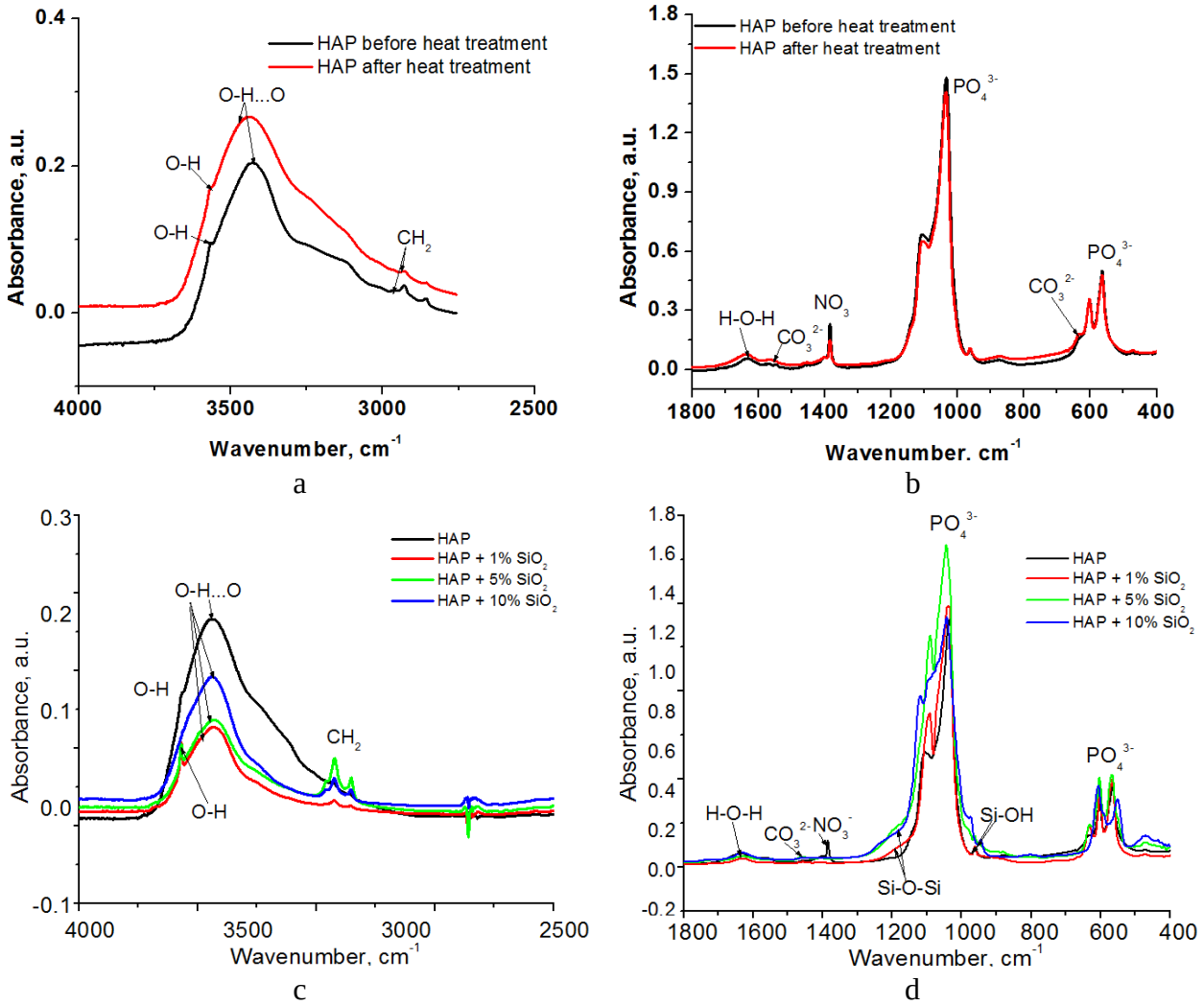

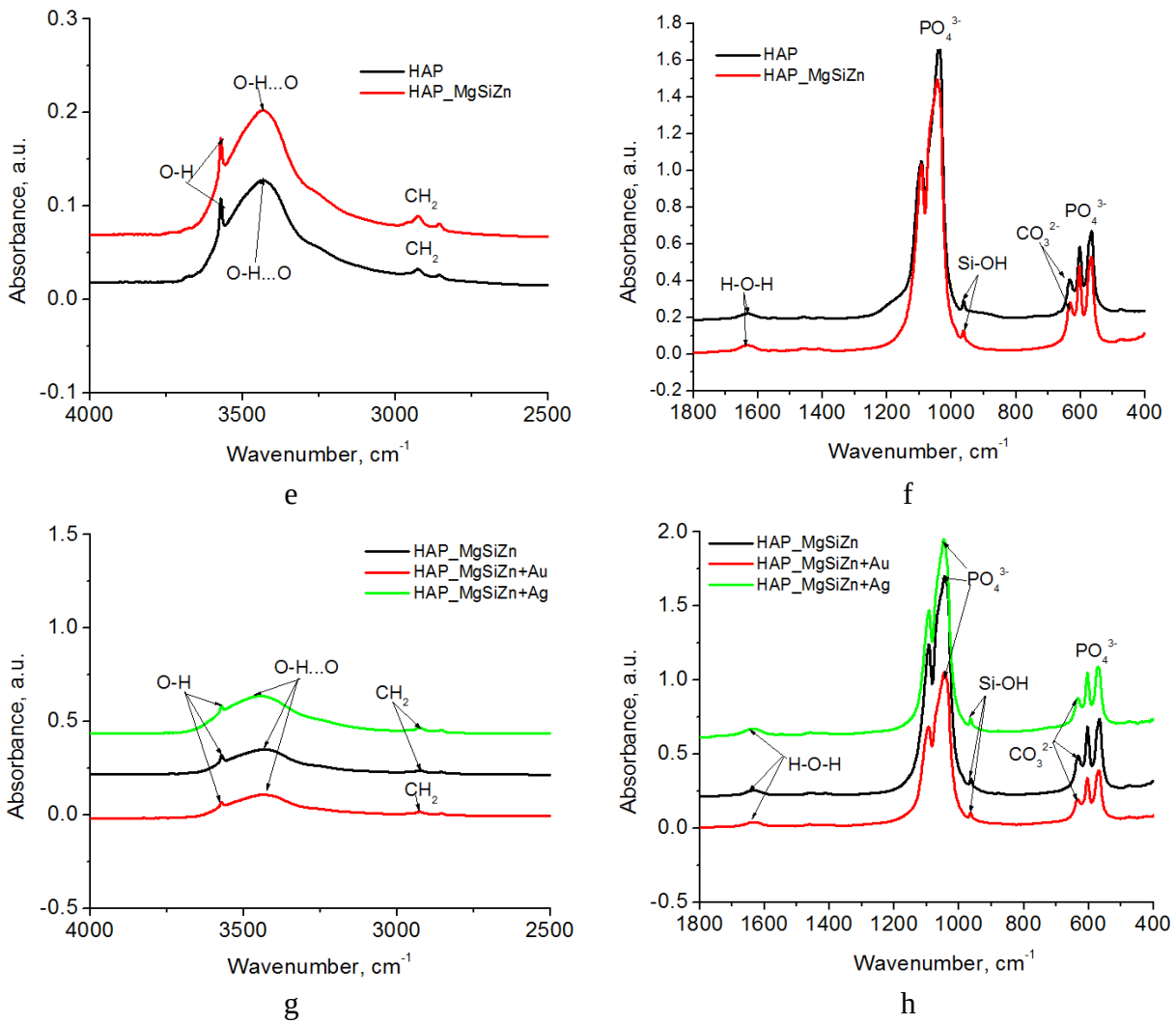


Figure 3.11 a-h. FTIR spectra of HAP before and after heat treatment at 650C °, HAP with 1%, 5%, 10% $SiO_2$, HAP_MgSiZn, HAP_MgSiZn+Au and HAP_MgSiZn+Ag after heat treatment at 650C° for the spectral ranges 4000-2500 $cm^{-1}$ and 1800-400 $cm^{-1}$.

Figure 3.11 a, c and g shows specific bands of hydrogen bridges in the OH..O groups at 3426 $cm^{-1}$ – 3438 $cm^{-1}$ in all the HAP samples studied. At 3566 $cm^{-1}$ appear the free OH groups on the surface of HAP particles for all samples. Figure 3.11 b shows the existence of $NO_3^-$ groups at 1380 $cm^{-1}$ for HAP samples without heat treatment, where there is a higher content of impurities than in the HAP sample treated at 650°C. Thus it appears that heat treatment decreases impurities in the sample. At 1463 $cm^{-1}$ appear specific bands for $CO_3^{2-}$, pointing out that phosphates absorb $CO_2$ from atmospheric air. The bands at 1090 $cm^{-1}$, 1030 $cm^{-1}$ and 960 $cm^{-1}$ correspond to $PO_4^{3-}$ vibrations. The FT-IR spectrum in Figure 3.11 d shows two characteristic bands: one at 980 $cm^{-1}$ attributed to the Si-OH vibration in silanol groups, and the 1100 $cm^{-1}$ band

corresponding to the–Si-O-Si- vibration from siloxane link. Their presence is due to the introduction into the system of $SiO_4^{4-}$ ions, which entering in the structure of hydroxyapatite form silanol and siloxane bonds.

### 3.2.3 X-ray diffractometry

By X-ray powder diffraction we determined the crystallinity degree of the powders and the crystallites size in the particles [233]. In figure 3.12 a-c are shown the X-ray powder diffraction patterns of samples HAP, HAP_MgSiZn, HAP + 5% $SiO_2$, HAP + 10% $SiO_2$, HAP_MgSiZn+Ag and HAP_MgSiZn+Au. All samples were calcined at a temperature of 650° C for 6 hours.

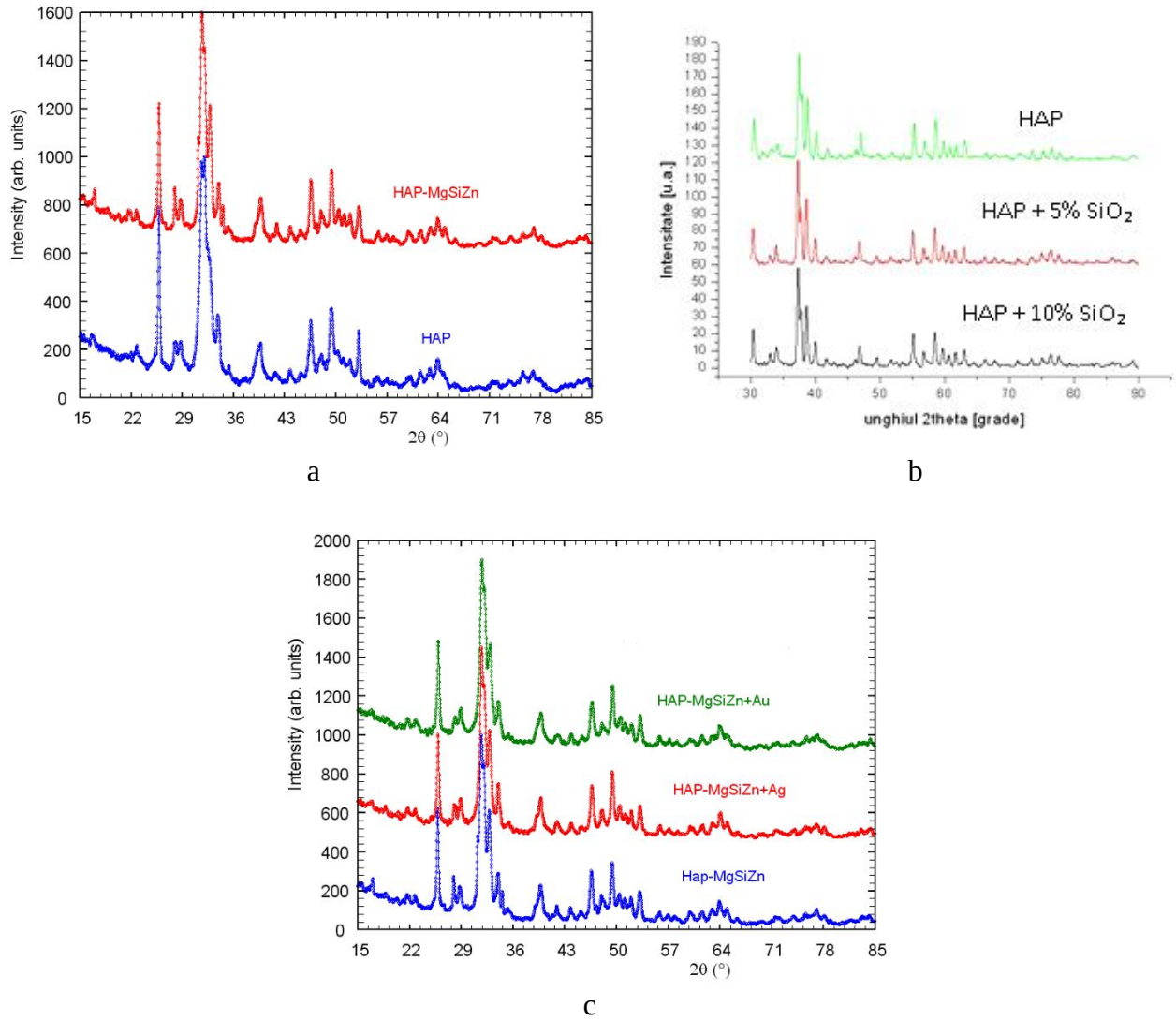


Figure 3.12 X- Ray powder diffraction patterns of samples: HAP and HAP_MgSiZn (a); X-RPD of HAP, HAP + 5% $SiO_2$ and HAP + 10% $SiO_2$ (b); X-RPD of HAP_MgSiZn+Ag (c).

From Figure 3.12 (a) and (c) of X-RPD it can be seen that there is no structural difference between the pure HAP and HAP_MgSiZn samples. The introduction of substitute ions into the hydroxyapatite system does not change its structure. Similarly we can say about the samples from Figure 3.12 (b), that the $SiO_4^{4-}$ ions introduced into the HAP in different proportions do not affect its structure. In these figures, peaks for $Mg^{2+}$, $SiO_2$ and $Zn^{2+}$ are not evidenced, because of their low concentrations in the structure of HAPs.

### 3.2.5 BET analysis

To highlight how the porosity and specific surface area influence the osteoblast behavior in cell cultures, we performed a BET analysis of the samples, after calcination at different temperatures. The results for samples prepared under various conditions of work are presented in Table 3.6.

Table 3.6 BET analysis of HAP samples with different compositions and concentrations, calcined at different temperature ranges:

| No. | SAMPLE | Specific surface area ($m^2g^{-1}$) | Porosity ($cm^3/g$) | Calcination tempera-ture °C |
|---|---|---|---|---|
| 1 | HAP standard Aldrich | 67.81 | 0.14 | - |
| 2 | HAP | 61.22 | 0.15 | - |
| 3 | HAP | 44.83 | 0.05 | 400 |
| 4 | HAP | 25.11 | 0.05 | 650 |
| 5 | HAP | 19.23 | 0.05 | 950 |
| 6 | HAP + 1%$SiO_2$ | 69.22 | 0.15 | 400 |
| 7 | HAP + 1%$SiO_2$ | 59.12 | 0.12 | 650 |
| 8 | HAP + 1%$SiO_2$ | 38.12 | 0.10 | 950 |
| 9 | HAP + 5%$SiO_2$ | 96.14 | 0.21 | 400 |
| 10 | HAP + 5%$SiO_2$ | 76.12 | 0.21 | 650 |
| 11 | HAP + 5%$SiO_2$ | 50.25 | 0.06 | 950 |
| 12 | HAP + 10%$SiO_2$ | 112.78 | 0.20 | 400 |
| 13 | HAP + 10% $SiO_2$ | 92.13 | 0.13 | 650 |
| 14 | HAP + 10% $SiO_2$ | 77.56 | 0.08 | 950 |
| 15 | HAP_0,28%$SiO_2$_0,67%Mg_0,2%Zn | 104.51 | 0.19 | 400 |
| 16 | HAP_0,28%$SiO_2$_0,67%Mg_0,2%Zn | 54.18 | 0.07 | 650 |
| 17 | HAP_0,28%$SiO_2$_0,67%Mg_0,2%Zn+ 0.14%Ag | 110.78 | 0.35 | 650 |
| 18 | HAP_0,28%$SiO_2$_0,67%Mg_0,2%Zn + 0.3%Au | 131.64 | 0.46 | 650 |

Data analysis in Table 3.6 shows that substituent ions as well as calcination temperature influence strongly the surface area and porosity of samples. The highest differences as compared to pure HAP samples are found in the samples containing $SiO_2$. Whith higher $SiO_2$ content the porosity and surface area increase. Calcination temperature strongly influences the surface area, which decreases with increasing temperature. The influence of temperature is most pronounced in samples with high $SiO_2$ content. Comparing pure HAP with partially substituted HAP samples, we find differences in specific surface area as high ea 100% or even more. The data in the table show that porosity and average pore radius are also strongly influenced by the $SiO_2$ content and especially by the calcination temperature. With increasing calcination temperature increases the pore radius, because at high temperatures the micropores present in the structure are destroyed.

### 3.2.6 TG, DTG, DTA, DSC analysis

Some are shown in Figure 3.17. The TG-DTA analysis shows that, with increasing temperature, mass loss increases as a result of water loss and decomposition of calcium and magnesium carbonates, producing the corresponding oxides, which determine the basic character of the aqueous suspensions of hydroxyapatite bioceramics. The analysis of diagrams from Figures 3.17 a-b reveals the complexity and large number of compounds and phases that are formed. Thus in the temperature range 20°C-300°C, for pure HAP a total mass loss of 7.17% is registered, from which 3.83 % corresponds to physically bonded water, while the remaining 3.34% water from hydrated calcium phosphates. In the temperature range of 300°C-600°C mass losses are only 0.43% and are assigned of decomposition of thermally more stable hydrates of calcium phosphate. A significant loss of 3% is visible in the temperature range of 600°C-820°C with two maxima on the DTG curve, related to magnesium carbonate, and respectively calcium carbonate decomposition at 800°C. The DTA curve in the temperature range of 600°C-800°C shows two exothermic peaks. In the temperature range of 810°C to 1200°C weight loss is only of 0.32%, corresponding to the scission of surface OH groups, with water elimination. DTA and DSC curves also show a strong endothermic process at about 1050°C, related to the of tetracalcium phosphate $Ca_4 (PO_4)_2O$:

$$Ca_4 (PO_4)_2O \rightarrow Ca_3 (PO_4)_2 + CaO$$

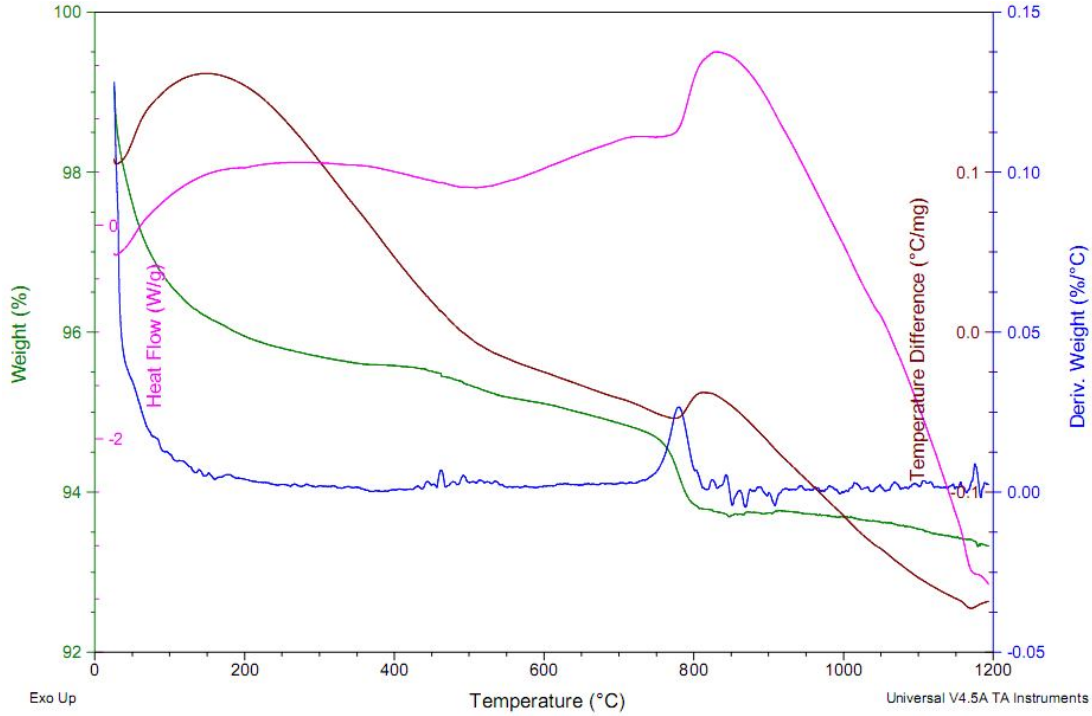


a

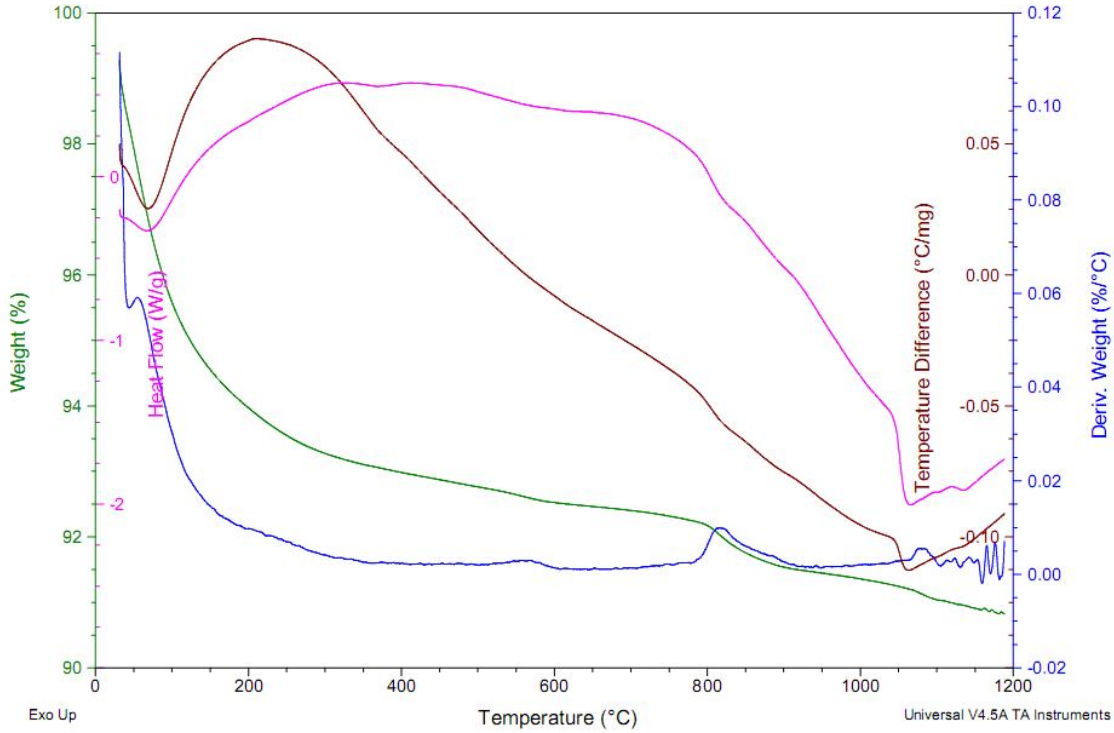


b

Figure 3.17 Thermograms of HAP 650 sample (a), and of HAP_MgSiZn 650 sample (b) (10 ° / min).

### 3.2.7 TEM imaging

From TEM images, both HAP particles morphology and their size can be determined. In Fig. 3.19 TEM images are presented for unsubstituted HAP powder calcined at 650$^{o}$C. In Fig. 3.22 are given TEM images of silver nanoparticles.

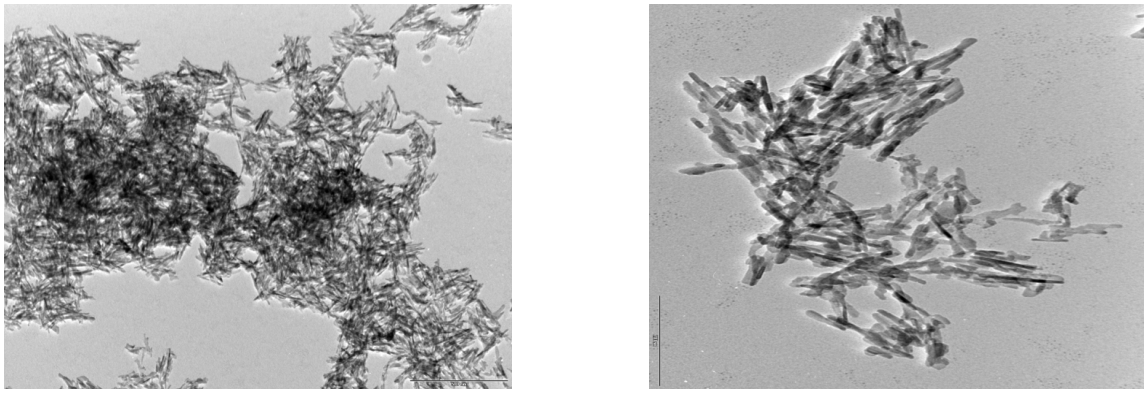

a b

Figure 3.19 TEM images of pure HAP particles calcined at 650°C; bars in the figure correspond to 500 nm (a) and 200 nm (b).

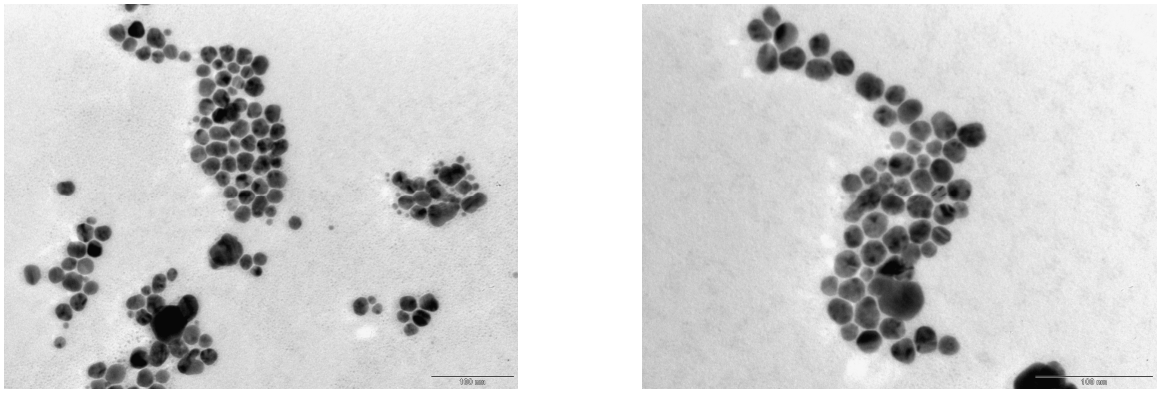

a b

Figure 3.22 TEM images of silver nanoparticles prepared by us. Bars of the images correspond to 100 nm.

In the TEM images of the pure HAP sample (Figure 3.19) small acicular particles 7-15 nm of are seen, with about 10 nm in diameter, and up to 100 nm lengths. Figure 3.22 shows TEM images of silver nanoparticles with sizes below 100 nm .

### 3.2.9 AFM imaging

For instance, AFM images in Figure 3.25 characterize the surface of non substituted s hydroxyapatite, calcined at 650° C.

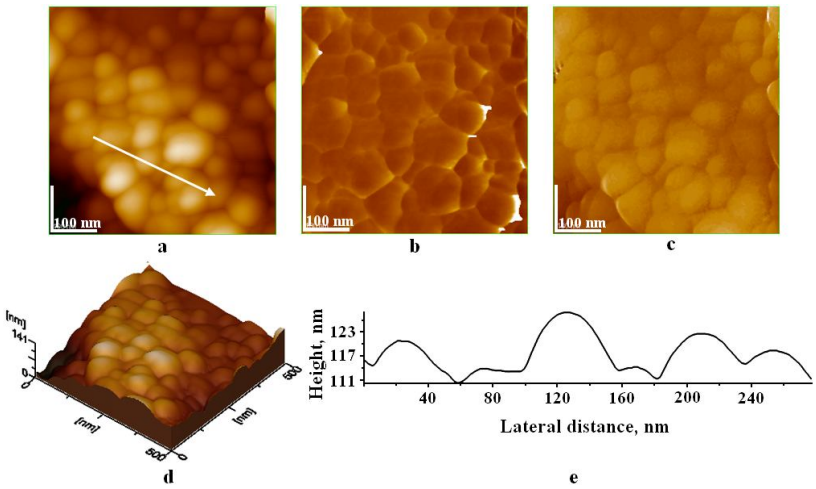


Figure 3.25 AFM images of HAP powder calcined at 650°C. Scanned area: 100 nm x 100 nm) 2D topographic image, b) phase image, c) amplitude image, d) 3D topographic image, e) cross section along the arrow in panel a.

Table 3.9 Average particles diameters determined from cross sections of AFM images.

| No. | Hydroxyapatite sample | Average particle diameter determined from cross section (nm) |
|---|---|---|
| 1 | Pure HAP | 24 |
| 2 | HAP + 10% $SiO_2$ | 40 |
| 3 | HAP_MgSiZn | 80 |
| 4 | HAP_MgSiZn + Ag | 35 |

Analyzing the data in Table 3.9, it is evident, that the smallest particles are those of for pure HAP (24 nm diameter). This is possible because the particle growth process was blocked by surfactant nonylphenol introduced in synthesis, which is adsorbed on the surface of particles and stops the further growth of particles.

## 4. PREPARATION OF NANOSTRUCTURED COMPOSITES

The latest advances in biomedical research relates to composite materials (biocomposites) processed at nanoscale. In studies undertaken in this work, we aim to assemble collagen and chitosan with hydroxyapatite to obtain biocomposites with a structure and composition as close as possible to that of natural bone. In this context, we prepared a partially substituted hydroxyapatite with $Mg^{2+}$, $Zn^{2+}$ and $SiO_4^{4-}$ ions as noted in Chapter 3, and assembled these particles on collagen fibers and chitosan to obtain biocomposites with structure and composition comparable to those of natural bone [257]. In Table 4.1 are presented the sorts of biocomposites prepared with hydroxyapatite, chitosan and collagen.

Table 4.1 Biocomposites prepared with hydroxyapatite, chitosan and collagen.

| **Sample** | **Components, additives and preparation** | | | | |
|---|---|---|---|---|---|
| | **M 650 = HAP_ 0,28%$SiO_2$_0,67 %Mg_0,2%Zn (%)** | **COLLAGEN (%)** | **CHITOSAN (%)** | **GLUTARALDEHYDE (GA)** | **Preparation medium** |
| **B1** | 73 | 27 | - | - | Acid |
| **B6** | 73 | 27 | - | - | Basic |
| **B2** | 93 | - | 7 | - | Acid |
| **B3** | 68.5 | 26 | 5.5 | - | Acid |
| **B4** | 75 | 24.5 | - | 0.5 | Acid |
| **B5** | 75 | 24.5 | - | 0.5 | Basic |

### 4.4.1 FTIR spectroscopy

FTIR spectra of materials COL, CHI, HAP_MgSiZn, HAP_MgSiZn +CHI /$SiO_2$, HAP_MgSiZn +COL /$SiO_2$ and HAP_MgSiZn +CHI /$SiO_2$+ COL /$SiO_2$ are shown in Figure 4.4 a-f. Based on these spectra we can do several considerations on the interactions that occur between phases of the system.

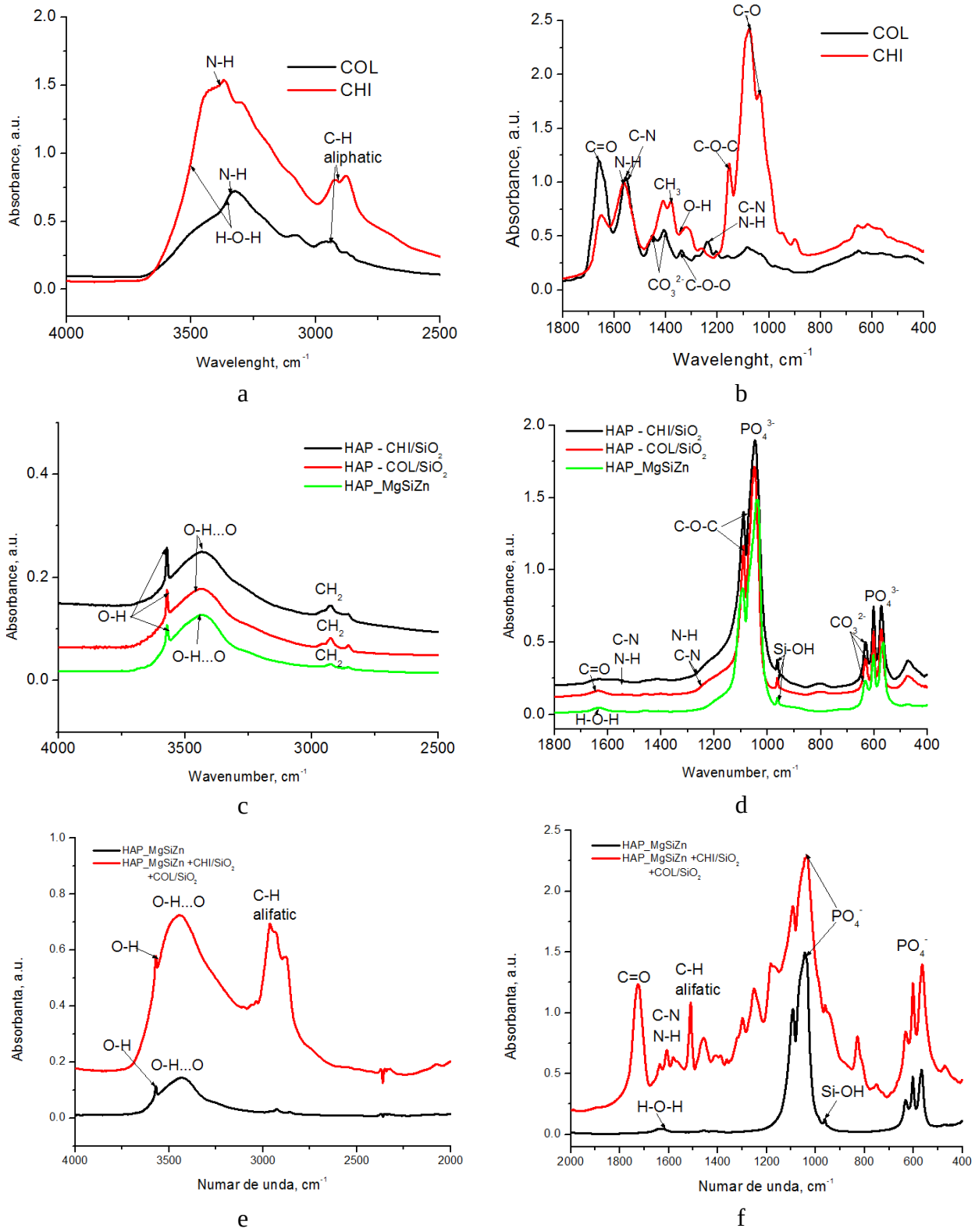


Figure 4.4 FTIR spectra of samples CHI, HAP_MgSiZn, HAP_MgSiZn +CHI /$SiO_2$ (a) and (b); COL, HAP_MgSiZn, HAP_MgSiZn +COL /$SiO_2$ (c) and (d); HAP_MgSiZn , HAP_MgSiZn +CHI /$SiO_2$+ COL /$SiO_2$ (e) and (f).

For **collagen** (consisting of 33% glycine and 22% proline or hydroxyproline) based on literature data [264], we have the following assignments: at 3433 $cm^{-1}$ H-O-H group (stretching) and at 2925 and 2858 $cm^{-1}$ C-H – (stretching vibration). At 1656 $cm^{-1}$ C=O stretching vibration band from amide I, and at 1542 $cm^{-1}$ the combination of N-H bending vibrations and C-N stretching from amide II. At 1452 $cm^{-1}$ there are bands of $CH_3$ bending vibrations and at 1243 $cm^{-1}$ C-N stretching and N-H bending vibration from amide II.

**Chitosan**, from literature data [265] presents at high frequencies, at 3421 $cm^{-1}$ a vibration of H-O-H coupled with N-H, and at 2925 and 2858 $cm^{-1}$ the C-H stretching vibration. Amide I band (C=O) is located at 1637 $cm^{-1}$, and amide II (N-H) is located at 1564 $cm^{-1}$. At 1383 $cm^{-1}$ we identify the bending vibration of $CH_3$ group.

Based on literature data [262] we observe the vibrational frequencies specific to hydroxyapatite, located in the high frequency domain, assigned to H-O-H groups at 3426 $cm^{-1}$ from water, bounded by hydrogen bonds. At 3566 $cm^{-1}$ we observe the presence of free OH groups from the surface of particles. In the vibration range from 2800-2925 $cm^{-1}$ we identify minimum absorption bands, assigned to $CH_2$ groups from the organic phase introduced in the synthesis as surfactant (nonylphenol). At 638 $cm^{-1}$ appear specific bands for the $CO_3^{2-}$ group originated from the ammonium bicarbonate added in synthesis. The $PO_4^{3-}$ vibration frequencies are located in the low frequency range, at 1090 $cm^{-1}$, 1030 $cm^{-1}$ and 590 $cm^{-1}$.

### 4.5.2 Characterization by SEM imaging

In the pictures below fibrous nature of collagen, mineralized with hydroxyapatite nanoparticles, is evidenced.

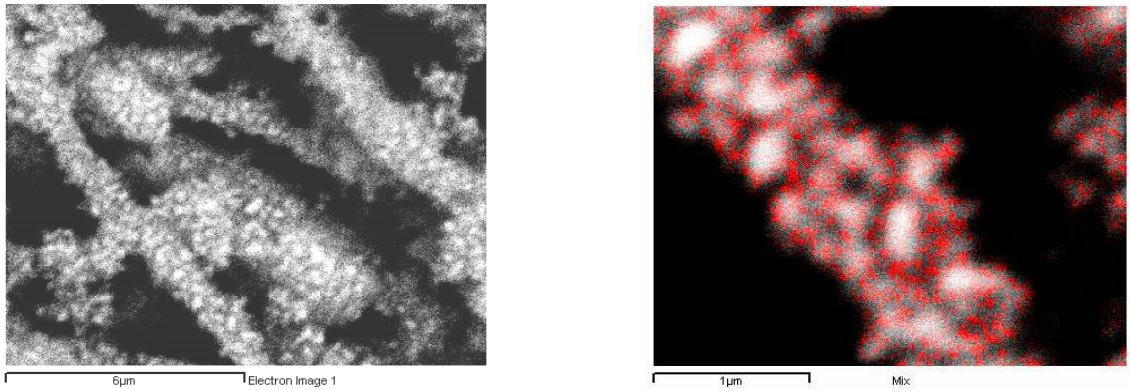


A b

Figure 4.11 SEM images of sample HAP_MgSiZn+COL/$SiO_2$ B1, (a) mineralized collagen fibers, (b) collagen fiber, superimposed $Ca^{2+}$ distribution

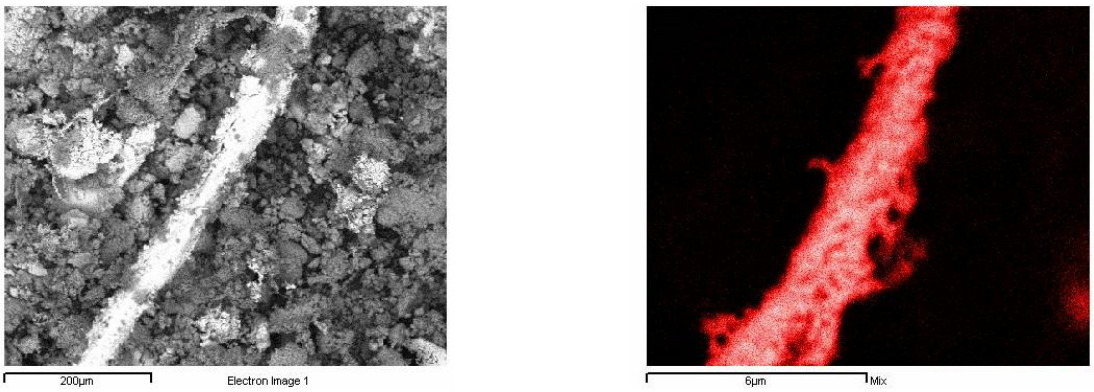


a b

Figure 4.12 SEM images of sample B6, (a) mineralized collagen fibers, (b) collagen fiber, calcium and phosphorus distribution.

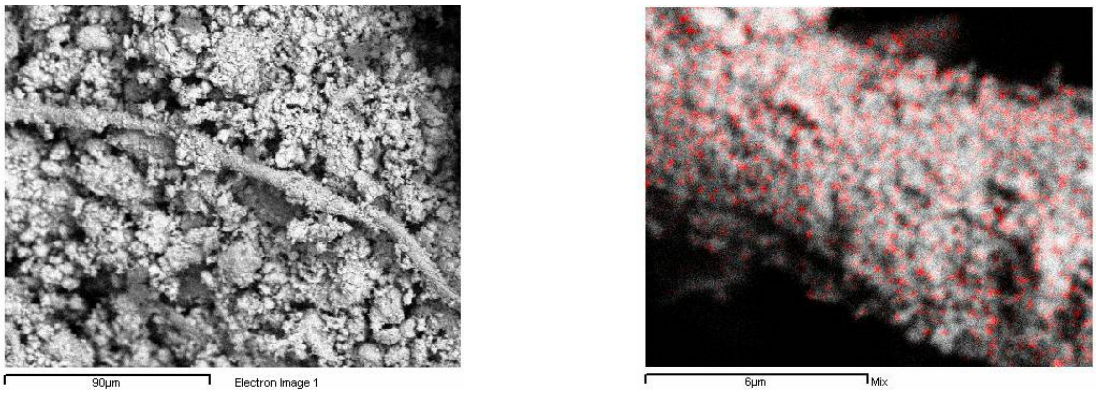


a b

Figure 4.13 SEM images of sample HAP_MgSiZn+COL/$SiO_2$ (acid medium+GA) (a) mineralized collagen fiber, (b) collagen fiber, superimposed $Ca^{2+}$ distribution.

### 4.5.3 Characterization by AFM imaging

A selection of AFM images of biocomposites particles is presented in Figures 4.17, 4.18 and 4.19. AFM images show different morphological structures of collagen fibers self-assembly with hydroxyapatite nanoparticles. This suggests that HAP nanoparticles lead to the formation of collagen self-assemblies with a high degree of stability. The interactions that occur between COL and nanoHAP can be explained by hydrogen bonds, but we do not exclude any simple mechanism of embedment of HAP nanoparticles in collagen matrix.

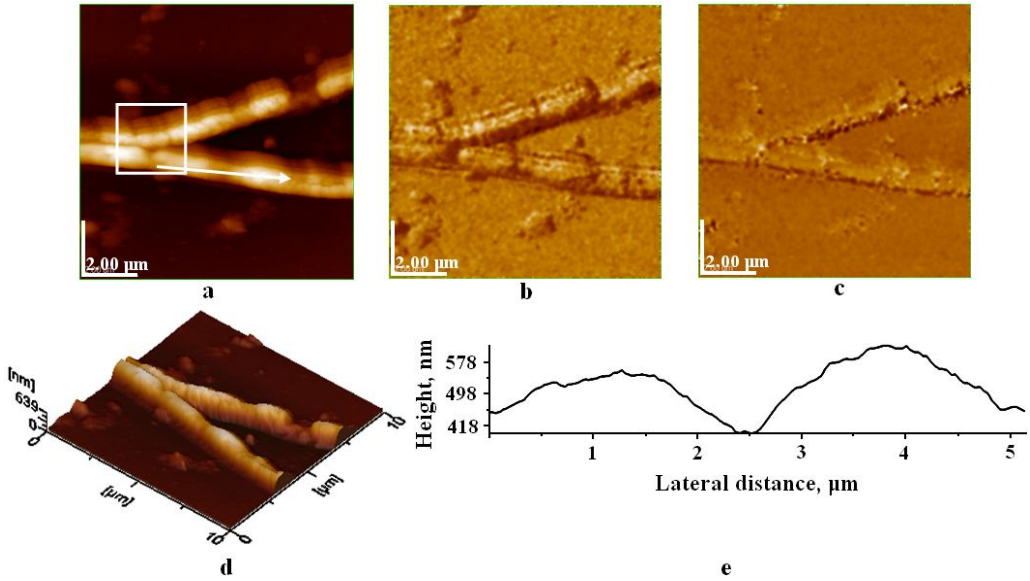


Figure 4.17 AFM images of mineralized collagen fiber. Scan area 2 mm x 2 mm, a) 2D topographic image b) phase image, c) amplitude image d) 3D topographic image e) longitudinal section along the arrow in panel a.

## 4.8 PREPARATION OF SCAFFOLDS FROM COMPOSITE MATERIALS

For scaffolds preparing the layer by layer technique was used for the deposition of hydroxyapatite with collagen and chitosan on ITO glass support. Here only the best method for obtaining the scaffolds is presented. It was found after numerous attempts to obtain the scaffold with optimum features regarding: chemical stability, morphology, chemical composition and design. So we used aqueous suspensions of 1 wt % HAP with different compositions and structures, 0.3 wt % COL solution and 2 wt % CHI solution. On the optical glass, treated with 5% HCl for 1 hour, activated with silicon ions, we deposited by vertical adsorption (immersions) successive layers of 5% sodium silicate - HAP - sodium silicate - CHI - sodium silicate - COL. After each deposited layer, five successive washing operations were executed, and drying was realized at room temperature, for 30 minutes / layer. Sodium silicate with 5% concentration was deposited to be the liant between the HAP, CHI and COL layers, in order to ensure a high chemical stability between layers. $SiO_2$ ions also confer a high and controlled porosity of scaffolds. The preparation scheme of scaffold is shown in Figure 4.40.

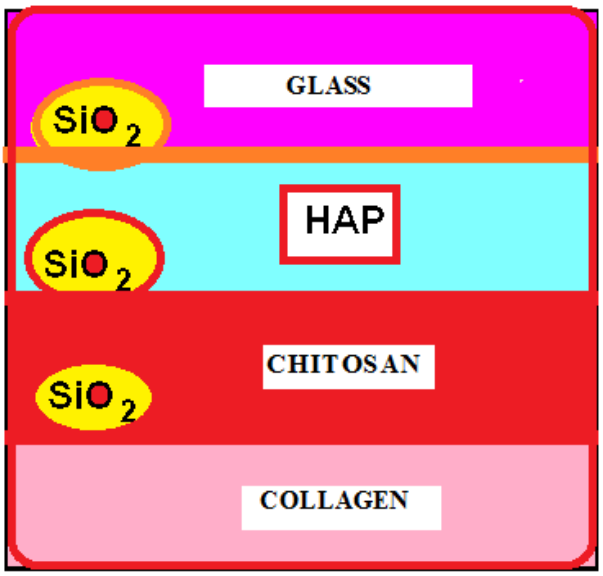


Figure 4.40 Scheme of scaffold preparation

## 4.9 SCAFFOLDS CHARACTERIZATION

### 4.9.1 AFM imaging

Scaffolds prepared by the layer by layer technique described above, were investigated on the surface by AFM imaging. The AFM images given in the Thesis present several kinds of our scaffolds, with different structures and morphologies, for instance the scaffold made of pure HAP + $SiO_2$ + CHI + $SiO_2$ + COL (Fig. 4.41), or the scaffold based on HAP with silicon (Fig. 4.42).

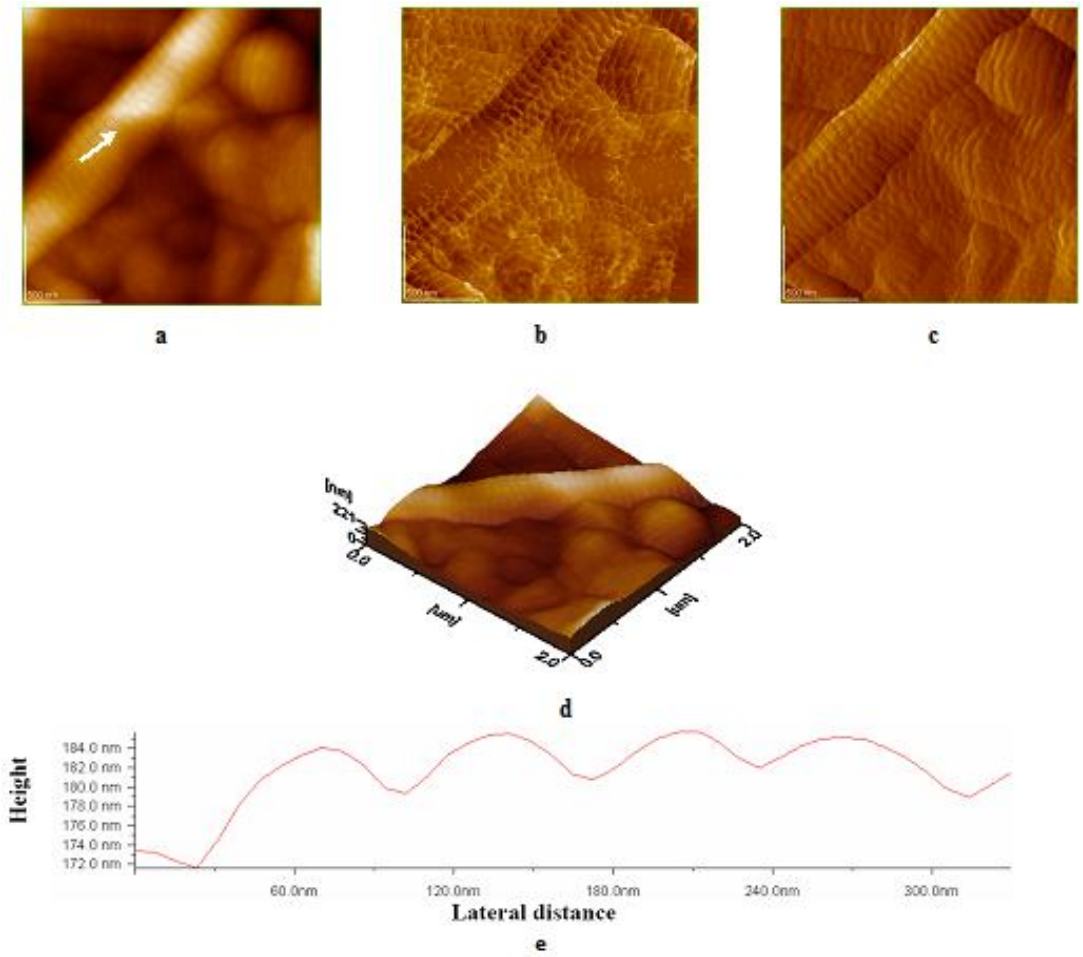


Figure 4.41 AFM images of the surface of the scaffold made of pure HAP + $SiO_2$ + CHI + $SiO_2$ + COL. Scan area 500 nm x 500 nm, a) 2D-topographic image, b) phase image, c) amplitude image, d) 3D-topographic image, e) cross section along the arrow in panel a.

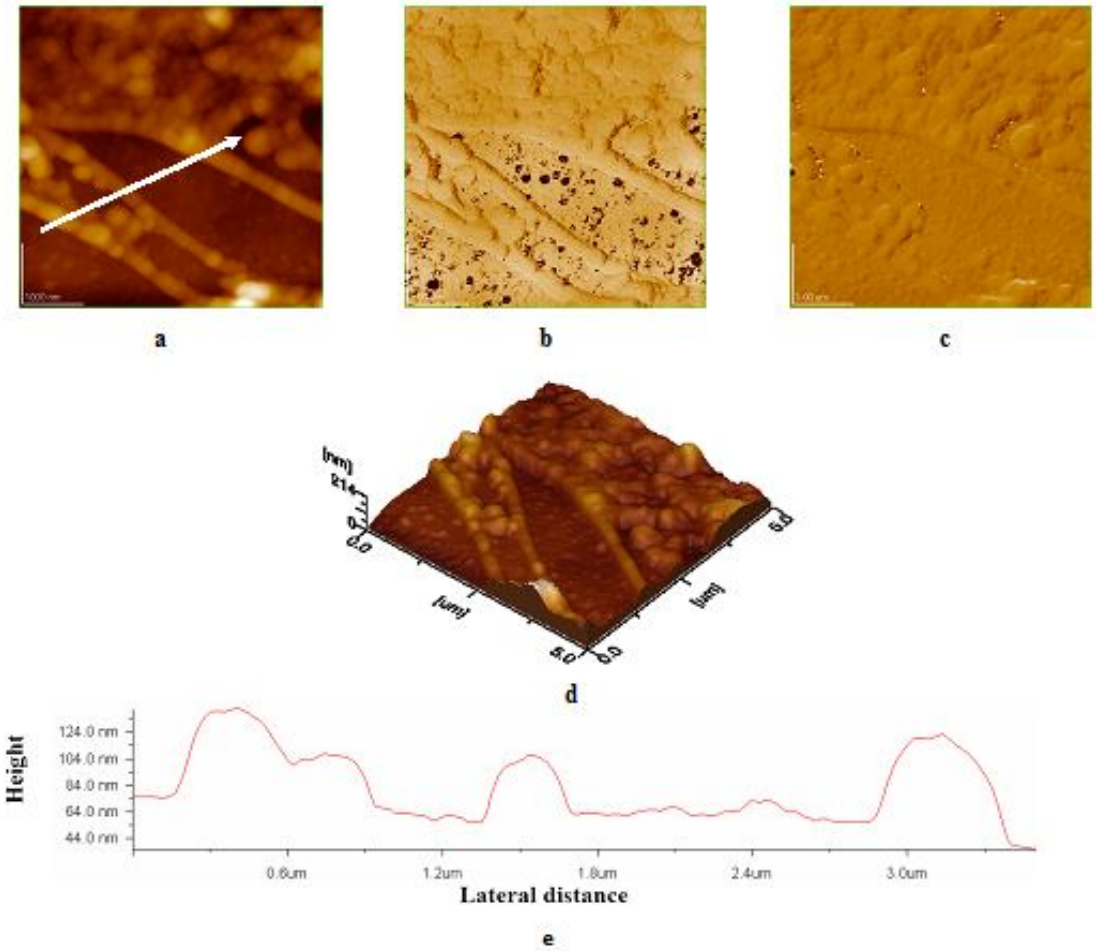


Figura 4.42 AFM images of the surface of the scaffold made of HAP+10% $SiO_2$ + $SiO_2$ + CHI + $SiO_2$ +COL. Scan area 500 nm x 500 nm, a) 2D-topographic image, b) phase image, c) amplitude image, d) 3D-topographic image, e) cross section along the arrow in panel a.

In the AFM images, o the scaffolds surface are observed mineralized collagen fibers with nanoparticles of hydroxyapatite (intrafibrilar mineralization), with a homogeneous distribution of them on ther surface.

## 5. THE BIOCOMPATIBILITY OF NANOSTRUCTURED COMPOSITES IN VITRO

### 5.2.1.1 Assessment of cell viability by MTT analysis

Investigation of osteoblasts cell proliferation is an important technique to assess the viability, biocompatibility and the toxicity of biocomposites on scaffolds *in vitro*.

The MTT assay (*3-(4,5-dimethylthiazol-2-yl)-2,5-diphenyltetrazolium bromide*) is based on the capacity of mitochondrial dehydrogenase to clive the tetrazole ring of MTT, yellow colored, in viable cells and to form dark blue formazan crystals, which cannot pass the cell membrane and are thus accumulated in vialable cells. The number of viable cells is proportional to the quantity of formazan formed. The solubilization of crystals is achieved by adding isopropanol, and the formazan quantity is determined by spectrophotometry at 492 nm wavelength.

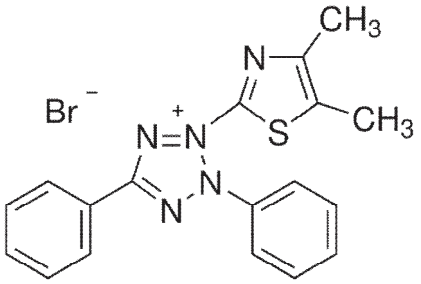


Figure 5.17 Chemical structure of MTT
3-(4,5-dimethylthiazol-2-yl)-2,5-diphenyltetrazolium bromide

Osteoblastic cells at passage 6 are detached from scaffolds with 0.25 % trypsin with the EDA for 5 minutes after 3 washes with PBS solution. Trypsin is inactivated by adding in culture medium 10% fetal serum. The suspension of cells is centrifuged for 5 minutes at 1000 rpm. Cell viability was checked by 0.4% tripan blue and the cells counting was performed with a Thoma hemocytometer.

The statistical analysis of results of the MTT assay was performed by Dunnett's multicomparison test. In this test we compared the control group (plastic) with each scaffold prepared with with HAP_ MgSiZn substrate; CHI substrate; COL substrate; HAP-MgSiZn + CHI + COL substrate.

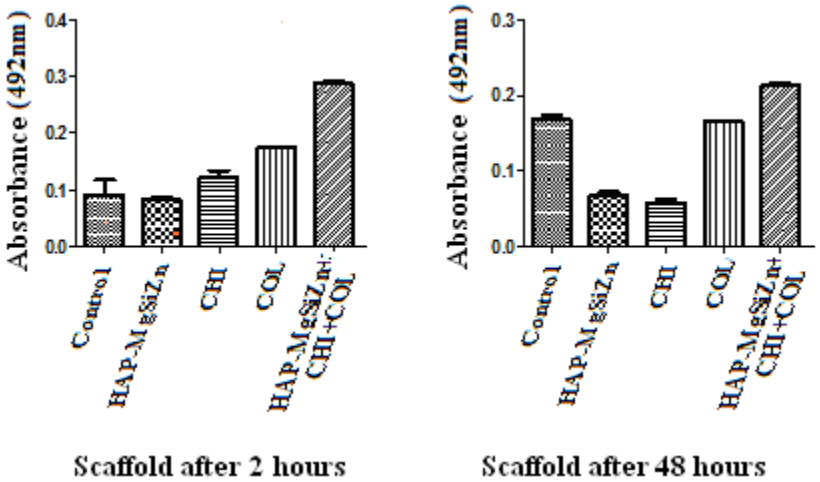


a b

Figure 5.18 MTT analysis of cells viability after 2 hours (a) after 48 hours (b) on scaffolds compared with the control sample (plastic) in identical culture conditions

From MTT analysis it can be seen, that cell adhesion on the scaffolds after 2 hours (Figure 5.18 a) is more intense than on the control scaffold. Absorbance values appear to be significantly different for scaffold with COL and the scaffold with HAP_MgSiZn + CHI + COL as compared with the control scaffold. The situation is the same after 48 hours (Figure 5.18 b). These significant differences are clearly influenced by scaffold composition, morphology and structure. The more complex the structure and composition of the scaffold is, the higher is the cells viability. The MTT assay shows that scaffolds have no toxic effect on cells and present a good biocompatibility with them.

#### 5.2.1.3 Immunocytochenical highlighting of molecules involved in cell adhesion

Osteoblasts contain specific molecules that are involved in cell adhesion phenomena, such as ***osteopontin and CD44 cell adhesion molecule.*** In our experiments we labeled with monoclonal antibodies the cells grown on scaffolds with substrate and on control scaffolds (plastic) to see if there are differences in expression of these antigens depending on the type of scaffolds (extracellular matrix) that are used.

**Investigation of scaffold: control with cells grown on a Petri dish treated with collagen type I at 3 days of culture**

Osteoblasts at passage 6 were seeded in osteogenic medium Promoocell culture for 3 days. Promocell differentiation medium is a medium containing specific factors that

induce the differentiation of bone. Immunocytochemical stains were performed for osteopontin, actin and DAPI.

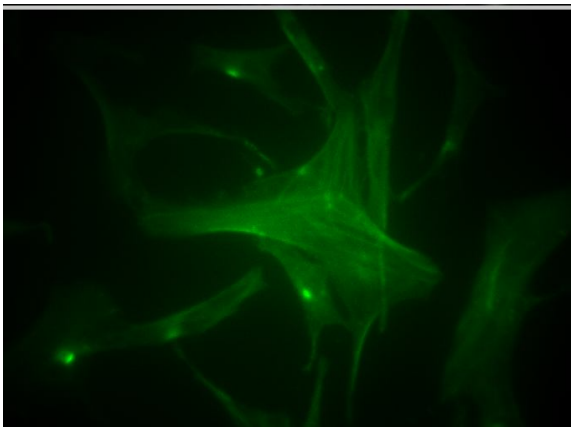

a.OP-FITC (x400)

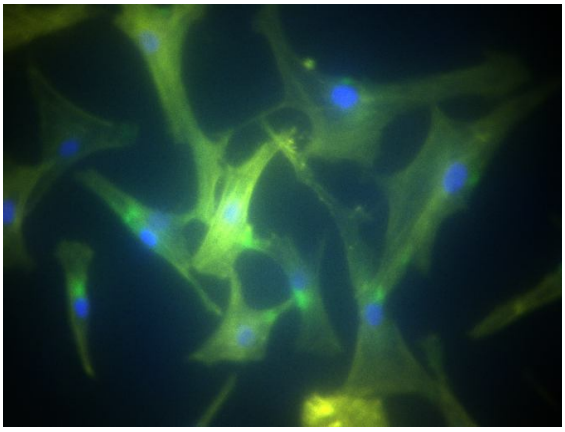

b. OP-FITC+ DAPI (x400)

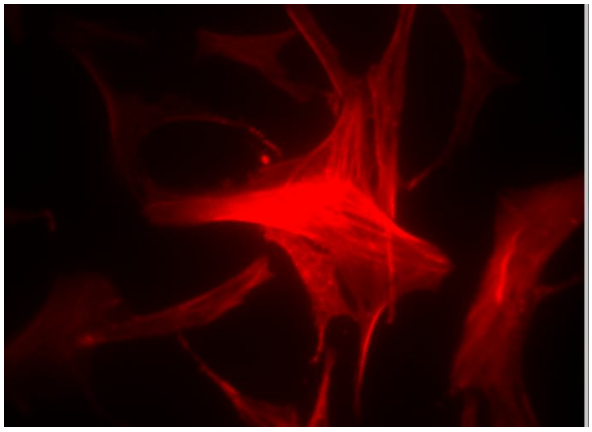

c. Faloidin –TRITC (x400)

Figure 5.20 Osteoblasts cells on control scaffold with collagen substrate, day 3.

Cells shows positivity for osteopontin (Figure 5.20 b). The morphology of cells at 72 hours is one for young cells, elongated, and with fibroblastoid character. Changes of citoskeleton resulting from adhesion of cells to plastic surface coated with collagen consisted in orientation of microfilaments of actin that are parallel to the longitudinal axis of the cells (Figure 5.20 c).

**Investigation of scaffold: HAP_MgSiZn + CHI/$SiO_2$ + COL/$SiO_2$ in cell culture medium at 7 days, dyeing - collagen FITC-TRITC-DAPI faloidin.**

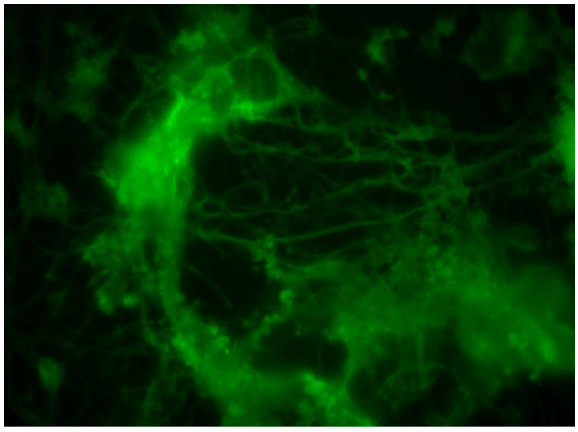

a

COL-FITC (x400)

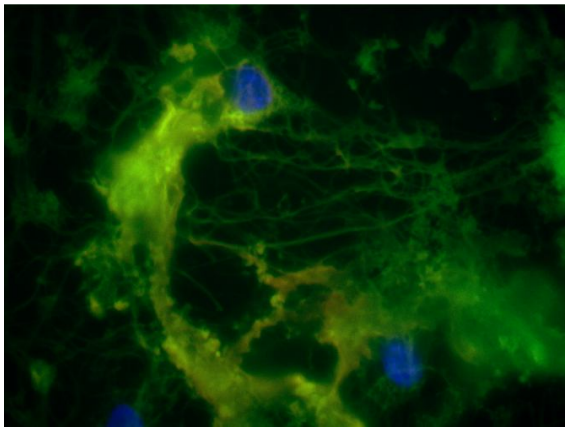

b

COL- FITC-faloidin TRITC-DAPI (x400)

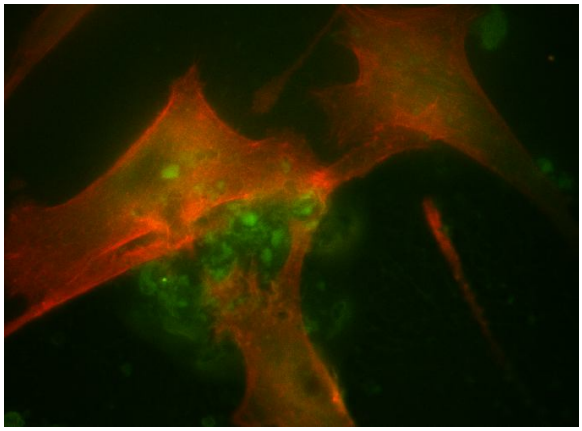

c

Triple staining: OP-FITC, faloidin TRITC, DAPI (x400)

Figure 5.23 a-c. Scaffold at 7 days of culture.

In this trial we aimed to highlight the *novo collagen* synthesis by osteoblastic cells. Unlike the control samples without cells, staining collagen fibers is more intense, these fibers are in direct contact with small cells and are covered by deposits of crystals of hydroxyapatite (Figure 5.23 b and c).

**Investigation of scaffold: HAP_MgSiZn + CHI/$SiO_2$ + COL/$SiO_2$ in cell culture medium at 3 days of culture.**

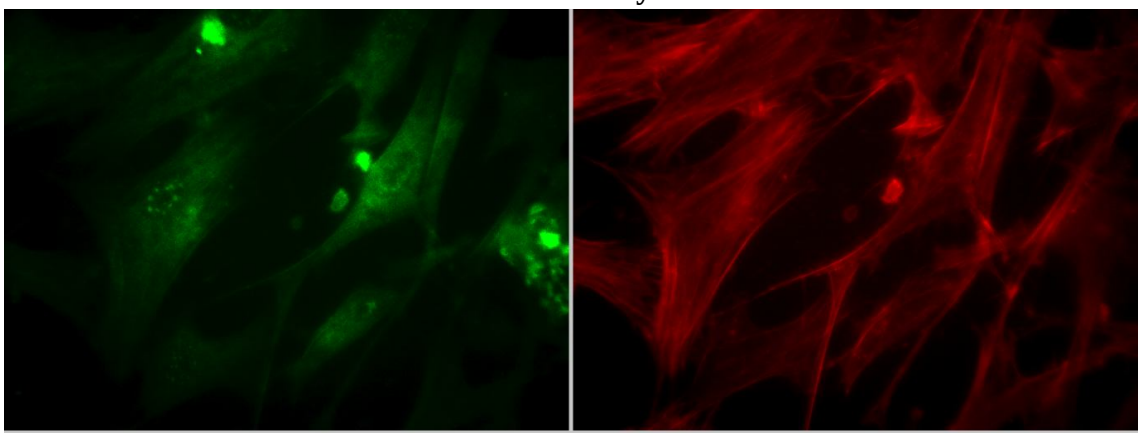

a. OP-FITC (x400) b. faloidin TRITC (x400)

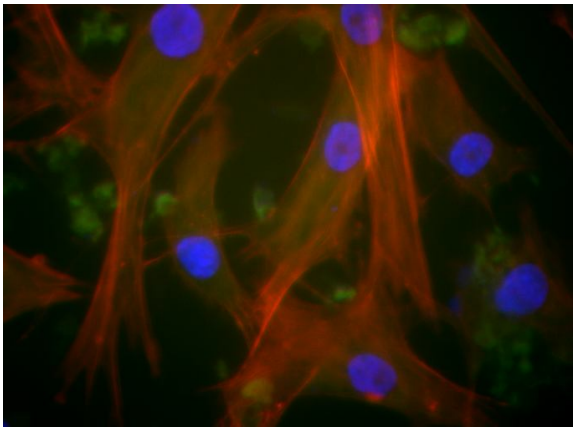

c Triple staining: OP-FITC + faloidin TRITC+ DAPI (x400);

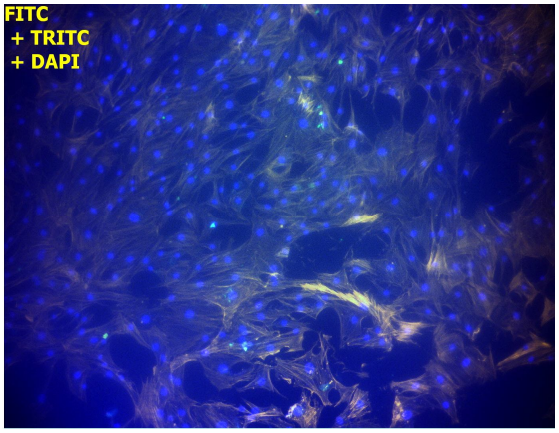


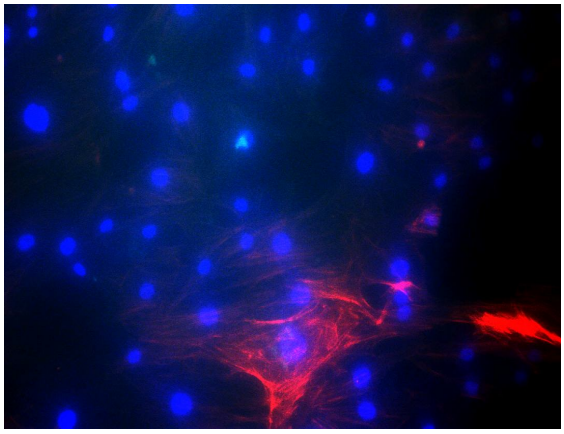

d. OP-FITC+Actin TRITC+DAPI (x200) e. OP-FITC+Actin TRITC+DAPI (x400)

Figure 5.24 a-e. Scaffold with cells in culture medium at 3 days.

Growing in standard culture medium for 3 days of osteoblasts on this scaffold induced a strong intracellular expression of osteopontin as compared with osteogenic medium Promocell cultivation (Figure 5.20 a-c). To notice is a younger cell morphology (elongated appearance) and increased density of actin filaments that are arranged in parallel fasces with the longitudinal axis of the cell (Figure 5.24 a and b). On the cell surface appear small hydroxyapatite crystals (Figure 5.24 c). Figure 5.24 (d) is a triple dyeing for OP-FITC, TRITC and DAPI actin-faloidin and Figure 5.24 (e) provides details of cytoskeleton, with the appearance of the stress fibers.

Osteoblasts behavior on 3D cultivation on matriceal supports differs according to structure and chemical composition of the scaffold substrate. An osteoinductive substrate induces high cells adhesion and proliferation and orients the cells to a more mature osteocyte cell phenotype (mature cell). The best results were obtained on matriceal supports containing modified hydroxyapatite with $Mg^{2+}$, $Zn^{2+}$, $SiO_4^{4-}$. Thus an accelarated cell proliferation was observed in a short time interval (3 days) on scaffolds, induced by the presence of these substituents in the structure, which positively influence the development of osteoblast cells..

Cell adhesion evaluation methods explored at this stage, namely assessing osteoblasts morphology, counting cells at different time intervals, immunocytochemical stains for proteins involved in adhesion process and in actin filaments showed significant differences between the scaffolds with different matrix preparations.

### 5.2.2 Investigation of scaffolds by SEM imaging

SEM imaging is a method to investigate the structure and surface of the scaffolds with or without cells. Thus we were able to observe the emergence of new structures on the scaffolds at certain time intervals and how the cells proliferate and develop on these.

Stages of the preparation of biological samples for SEM imaging were:

- fixing the samples with 2.5% glutaraldehyde;
- washing the samples with phosphate buffer (PBS);
- sputter-coating the samples with 6nm gold .

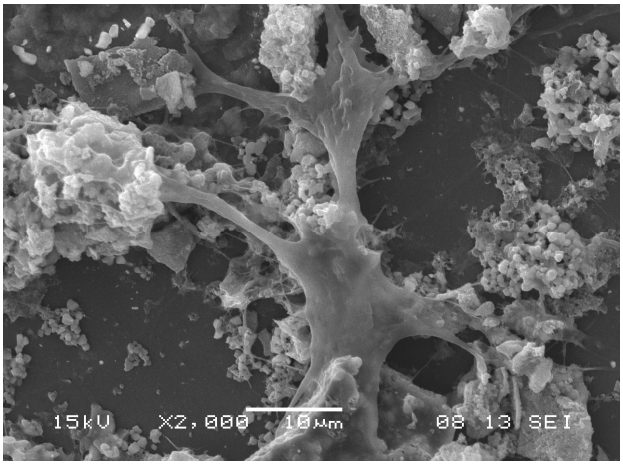


a

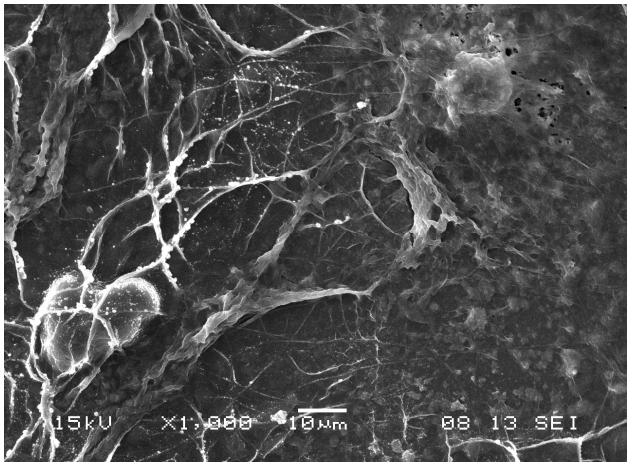


b

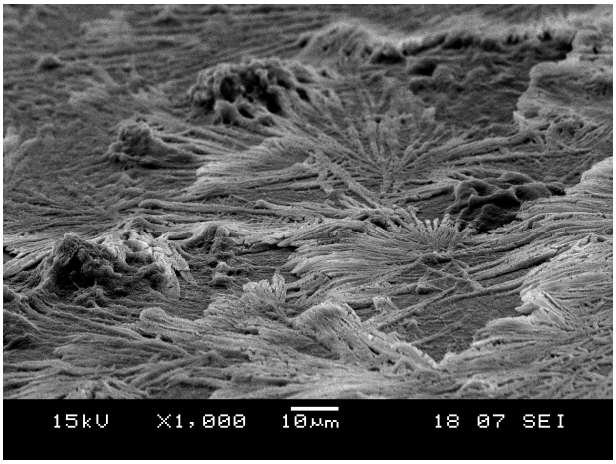


c

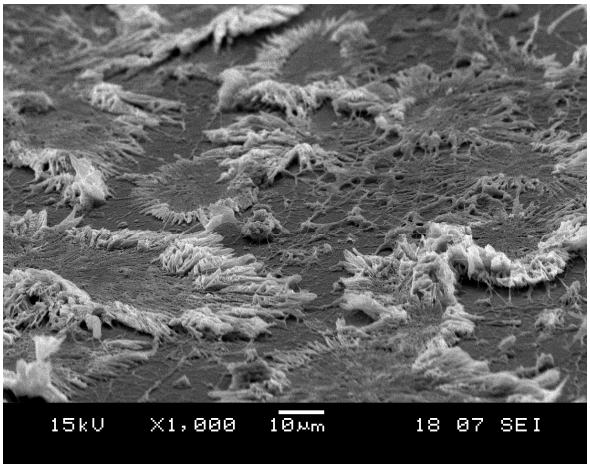


d

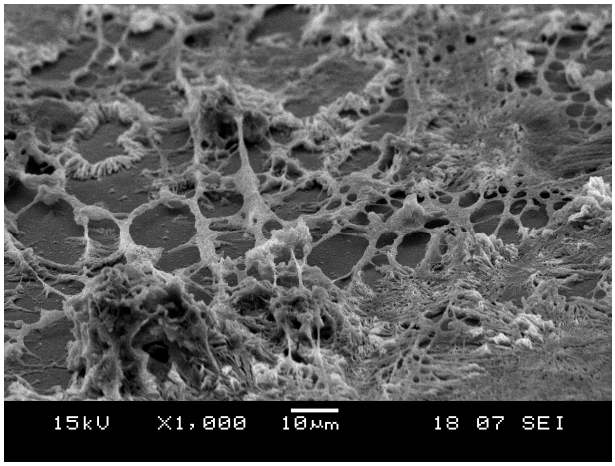


e

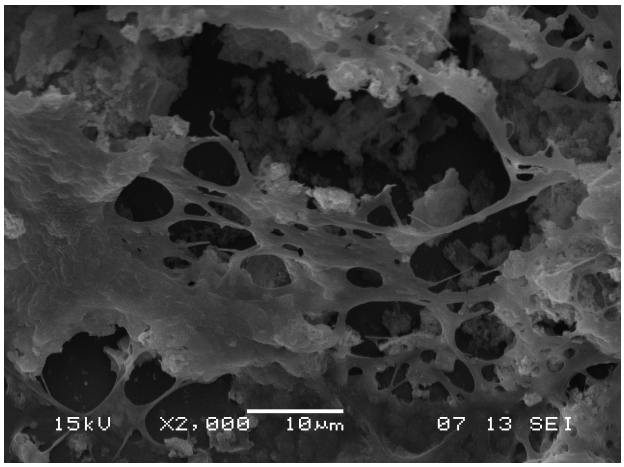


f

Figure 5.28 SEM images of scaffold HAP_MgSiZn + SiO2 + CHI + SiO2 + COL + cells at 3 days (a), (b) and 7 days of culture (c), (d), (e), (f).

In all SEM images a three-dimensional organization of scaffolds is evident, with induction of maturation (differentiation) of osteoblast cells to osteocyte cells with charactersitic features and dendritic extensions. In figure 5.28 e and f we observe in the intercellular space the existence of a proper matriceal network created by osteoblast cells, wuth *de novo* synthesis of bone matrix.

### 5.3 Visualization of osteoblasts by TEM imaging

Osteoblast cells viability testing was done by TEM imaging. To this end, cell detachment was performed after 7 days of culture, through a special method. Thus, the cells were detached from the scaffold by tripsinization and then centrifuged. A button cell is obtined, ehich is encapsulated in a special resin and then, by cutting the sample with a microtome, ultrafine sections of 40 nm are obtained.

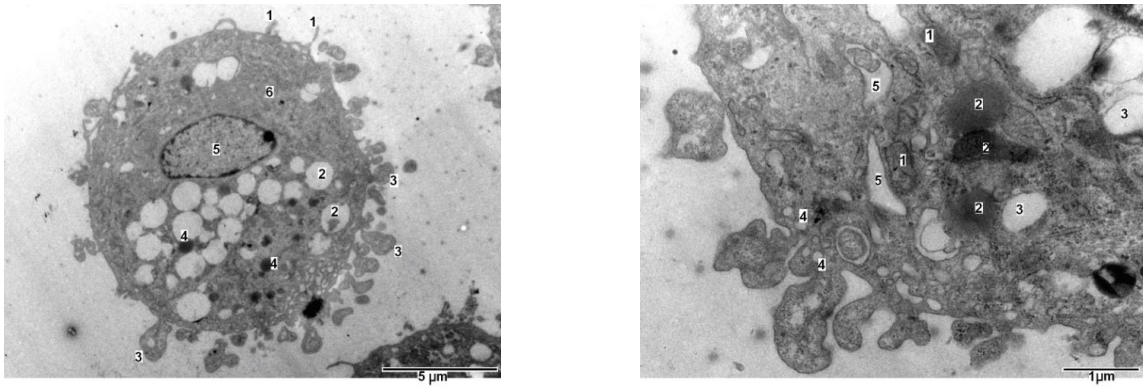


a b

Figure 5.35 (a). Cross-section through a cell with intense exocytosis processes (export from within to the extracellular environment). Microviles (1), vesicles (2), exocytated formations out of the cell (3), lysosomes (4) the cell nucleus (5), cytoplasm (6) (b). cross section through a portion of the cell: 1 - mitochondria, 2 - lysosomes, 3 - vesicles, 4 - microvesicles of endocytosis, 5 - REG. Both exocytosis and endocytosis processes are observed.

In TEM images presenting sections at various levels in the cell, we observe all important specific cellular organelles, and this is a prove of their excellent viability. For example, here are observed the nucleus, where DNA and RNA are synthesized; the nucleol which acts in cell preparation for mitotic cell division; the mitochondria which generate the most of the ATP - used as energy source in biochemical reactions in the cell. Also we see the presence of the endoplasmic reticulum (ER), where the biosynthesis of proteins and lipids takes place. In Figure 5.35 both processes of cell exocytosis and endocytosis of cell are seen. These all demonstrate, that the cell has intense biological activity, resulting in its remarkable viability.

### 5.2.6 SEM and EDX analysis of natural bone

In order to investigate the surface and chemical composition of natural bone, we made its SEM and EDX analysis, shown in Figure 5.37 a-d.

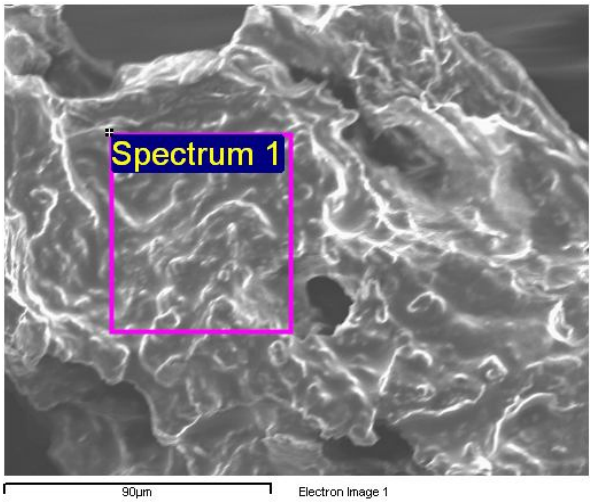


a

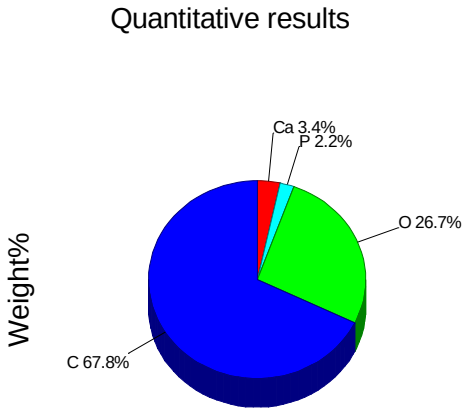


b

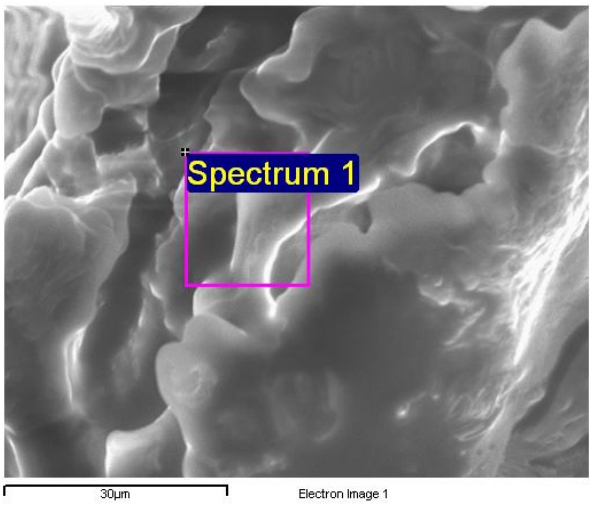


c

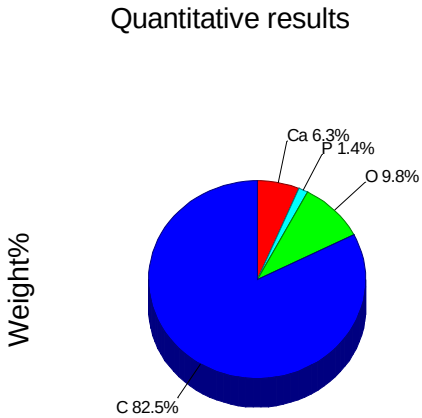


d

Figure 5.37 SEM image of natural bone (a) and (c); elemental chemical analysis of natural bone (b) and (d).

From the SEM images and EDX analysis of natural bone, its structure and chemical composition can be observed. The fragments of natural bone were obtained during a surgical intervention for the reconstruction of knee joint, with the patients's permision.

# 6. GENERAL CONCLUSIONS

- We carried out a synthesis and an analysis of the factors in kinetic equations for the formation and growth of nuclei and we highlighted the role of reactants concentration, of the pH of the reaction medium, and of the supersaturation on the particles size. We also determined the nature and amount of surfactants to be added in the synthesis.

- We established the order and manner of adding substituent ions to avoid the formation of α and β tricalcium phosphate.

- By experimental measurements we optimized the time duration of hydrothermal treatment (24 h) to bring the solid phase composition to the ratio $Ca/PO_4$ = 1.67, i.e. the ratio corresponding to hydroxyapatite.

- Using as surfactants starch, gelatin, whey from cow milk and nonylphenol, we have determined that nonylphenol is the best surfactant, followed by, which contains lactose and a series of proteins.

- We ascertained the optimum temperature of calcination to achieve the degree of crystallinity, an important factor for the materials used in orthopedics and dentistry, to range between 650°C and 750°C, a temperature interval where carbonates are not subject to thermal decomposition.

- We developed assembly methods for HAP/COL, HAP/CHI and HAP/CHI/COL, both in cements (biocomposites B1, B2 and B3) and as scaffolds, by adsorption on ITO glass surfaces by the layer by layer method, by successive vertical immersions in suspension of components.

- Hydroxyapatite prepared by our original method, partially substituted with $SiO_4^{4-}$, $Zn^{2+}$ and $Mg^{2+}$ ions in the proportions indicated in Chapter 3, showed the best biocompatibility with osteoblast cells, as compared with the other HAP and $SiO_2$ substituted HAP samples.

- By the way of experiments we ascertained the optimal conditions for scaffolds preparation, in order to ensure the best adhesion, cell proliferation and differentiation phenomena.

- The addition of 5% sodium silicate solution and controlling the pH, we obtained scaffolds with different morphologies and controlled porosity.

- Microstructures characterization was done by means of TEM, SEM and AFM microscopy, X-ray diffractometry, FTIR and XPS. The results showed that they have a structure with well defined crystallinity and particle size in the nanometer range.

- Introduction of silver at nano-scale (10 nm) in the HAP structure confers to HAP superior properties (such as adhesion, proliferation) in comparison to pure HAP (Figures 5.16 and 5.17).

- The analysis of optical microscopy images shows that on HAP nanostructures, partially substituted with $SiO_4^{4-}$, $Mg^{2+}$, and $Zn^{2+}$ ions, the adhesion phenomenon occurs more intensely since the first 3 days of culture of osteoblastic cells, as compared with pure HAP nanostructures.

- After 7 days in osteoblast cell culture medium, we found that the number of cells per unit area ($1mm^2$) decreases because adhesion is increasing, a process whcih is inverse proportional to the phenomenon of cell proliferation.

- Nanostructured HAP containing silver and gold shows biocompatibility properties just below those of complex HAP. This feature suggests that the use of HAP nanostructures that containing silver and gold should be preferred, due to their properties. Silver has the ability to tdestroy viruses and bacteria and gold nanoparticles have the potential to be used for the manufacturing of rapid diagnostic for theidentification of toxic agents, microbes or allergens in body fluids.

- TEM images presenting sections of various levels in the cell, reveal the presence of all important specific cellular organelles that demonstrating their excellent viability. Also by TEM imaging exocytosis and endocytosis processes of cell are evidenced, making obvious the high cell activity, resulting in its remarkable durability.

- EDX analyses of osteoblastic cells, natural bone and bone at the prosthesis interface reveal their chemical composition, similar to the chemical composition of the nanostructures that we have prepared in this thesis.

**SELECTIVE BIBLIOGRAPHY**


1. Temenoff J.S., Mikos A.G.; Injectable biodegradable materials for orthopedic tissue engineering; Biomaterials, 21: 2405-2412, 2000.

2. Kelly E.B.; New Frontiers in Bone Grafting; Orthopedic Technology Review, 2:28-33, 2000.

3. Crane G.M., Ishaug S.L., Mikos A.G.; Bone tissue engineering; Nature Medicine, 1:1322-1324, 1995.

4. Athanasiou K.A., Zhu C.F., Lanctot D.R., Agrawal C.M., Wang X.; Fundamentals of biomechanics in tissue engineering of bone; Tissue Engineering, 6:361-381, 2000.

204. Gravens D., Margraf H., Butcher H., Ballinger W.; The antibacterial effect of treating sutures with silver. Surgery, 73:122- 127, 1973.

205. Heard S.O., Wagle M., Vijayakumar E.; The influence of triple-lumen central venous catheters coated with chlorhexidine/silver sulfadiazine on the incidence of catheter-related bacteremia: a randomized; Controlled clinical trial. Arch Intern Med,158:81-87, 1998.

206. Kerker M.; The optics of colloidal silver: something old and something new; Journal of Colloid and Interface Science,105:297-314, 1985.

207. Liedberg H., Lundeberg T.; Silver alloy coated catheters reduce catheter-associialed bacteriuria. Br J Urol, 65:379-381, 1990.

208. Livingston-Wheeler V., Wheeler O.W.; The microbiology of cancer: Physician's Handbook; Spring Valley, CA: A Livingston-Wheeler Medical Clinic Publication, 1977.

209. Madden M.R., Nolan E., Finkelstein J.L, Yurt R.W, Smeland J., Goodwin C. W., Hefton J., Staiano-Coico L.; Comparison of an occlusive and a semi-occlusive dressing and the effect of the wound exudate upon keratinocyte proliferation; J.Trauma, 29:924-930, 1989.

210. Maki D.G., Cobb L., Garman J.K., Shapiro J.M,. Ringer M., Helgerson R.B.; An attachable silver-impregnated cuff for prevention of infection with central venous catheters: a prospective randomized multicenter trial. Am J Med, 85:307-314, 1988.

211. Maki DG, Stolz SM, Wheeler S, Mermel LA.; Prevention of central venous catheter-related bloodstream infection bz use of an antiseptic-irnpregnated catheter: a randomized. controlled study; Ann Intern Med; 127:257-266, 1997.

212. Margraf H.W, Covey T.H Jr; A trial of silver-zinc-allantoinate in the treatment of leg ulcers; Arch Surg, 112:699-704, 1977.

213. Morones J.R.; The bacteriocidal effects of silver nanoparticles; Nanotechnology, 16:2346-2353, 2005.

214. Moyer C.A., Brentano L., Gravens D.; Treatment of large human burns with silver 0.5% nitrate solution; Arch Surg, 90:812–867, 1965.

215. Niizeki K., Hashimoto K.; Treatment of molluscum contagiosum with silver nitrate; Paste. Pediatric Dermatology, 5:395–397, 1999.

216. Olson M.E., Wright J.B., Lam K.; Healing of porcine donor sites covered with silver-coated dressings; Eur J Surg, 166:486–489, 2000.

217. Cai L., Wang Q., Gu C., Wu J., Wang J., Kang N., Hu J., Xie F., Yan L., Liu,X., Cao, Y. , Xiao R. ; Vascular and micro-environmental influences on MSC-coral hydroxyapatite construct-based bone tissue engineering; Biomaterials, 32:8497-8505, 2011.

218. Russell A.D., Path F.R., Hugo W.B.; Antimicrobial activity and action of silver; Prog Med Chem., 31:354, 1994.

219.Sosa I.O., Noguez C., Barrera R.G.; Optical properties of metal nanoparticles with arbitrary shapes; Journal of Physical Chemistry B., 107:6269-6275, 2003.

223. Haghbin N. M., Solati-Hashjin M., Moztarzadeh F.; Preparation of hydroxyapatite ceramics for biomedical applications; Journal of Ceramic Processing Research, 10:54-57, 2009.

224. Faming Z., Jiang C., Jianxi L., Kaili L., Congqin N.; Bioinspired structure of bioceramics for bone regeneration in load-bearing sites; Acta Biomaterialia, 3:896–904, 2007.

225. Sung-Baek C., Fumiaki M., Tadashi K., Kazuki N., Naohiro S., Takashi N.; Apatite-forming ability of silicate ion dissolved from silica gels; Journal of Biomedical Materials Research, 32:375-381, 1996.

226. Sz-Chian L., San-Yuan C., Hsin-Yi L., Jong-Shing B.; Structural characterization of nano-sized calcium deficient apatite powders; Biomaterials, 25 : 189–196, 2004.

228. Karin A. H., Peter A. R., Nigel S., Thomas B.; Effect of silicon level on rate, quality and progression of bone healing within silicate-substituted porous hydroxyapatite scaffolds; Biomaterials, 27:5014–5026, 2006.

229. Yoshinobu F., Hiroshi Y., Kunio K., Tsugio S. , Akitsugu O.; Preparation of needle-like hydroxyapatite by homogeneous precipitation under hydrothermal conditions; Journal of Chemical Technology & Biotechnology, 57:349 – 353, 2007.

230. Shigeru S., Takayuki Y., Toshihiro M., Hiromu H., John B. M.; Preparative enhancement of the thermal stability of calcium hydroxyapatites ; Journal of Solid State Chemistry, 142:319 -324, 1999.

231. Marı´a V. R, Daniel A.; Silicon substituted hydroxyapatites. A method to upgrade calcium phosphate based implants; J. Mater. Chem., 15:1509–1516, 2005.

232. Mahdi R., Fathollah M., Mohammadreza T.; Formation of hydroxyapatite nanoneedles on the surface of a novel calcium phosphate/blood plasma proteins biocement in simulated body fluid (SBF); Journal of Ceramic Processing Research, 10:669-673, 2009.

233. Anna S., Zofia P., Czesława P.; FTIR and XRD evaluation of carbonated hydroxyapatite powders synthesized by wet methods; Journal of Molecular Structure 744–747, 657–661, 2005.

234. Wang H.X., Guan S.K., Wang X., Ren C.X., Wang L.G. ; In vitro degradation and mechanical integrity of Mg–Zn–Ca alloy coated with Ca-deficient hydroxyapatite by the pulse electrodeposition process; Acta Biomaterialia, 6:1743-1748, 2010.

235. Dietrich E., Oudadesse H., Lucas-Girot A., Le Gal Y., Jeanne G. S. ; Effects of Mg and Zn on the surface of doped melt-derived glass for biomaterials applications; Applied Surface Science, 255:391-395,2008

236. Kim S. R., Lee J. H. , Kim Y. T., Riu D. H., Jung S. J., Lee Y. J., Chung S. C., Kim Y. H.; Synthesis of Si, Mg substituted hydroxyapatites and their sintering behaviors; Biomaterials, 24:1389-1398, 2003.

255. Mocanu A., Cernica I., Tomoaia Gh., Bobos L-D,, Horovitz O., Tomoaia-Cotisel M.; Self-assembly characteristics of gold nanoparticles in the presence of cysteine; Colloids and Surfaces A: Physicochem. Eng. Aspects, 338: 93–101, 2009.

256. Yogita G., Mathur G. N., Sandeep V.; Biomimetic synthesis and ultrastructural characterization of a zerovalent gold–hydroxyapatite composite; Bioorganic & Medicinal Chemistry Letters 16:363–366, 2006.

257. Barbu-Tudoran L., Tomoaia Gh., Horovitz O., Mocanu A., Tomoaia-Cotisel M., Self-assembly characteristics of gold nanoparticles in the presence of arginine; Journal of optoelectronics and advanced materials, 10: 2293 – 2297, 2008.

262. Sionkowska A., Kozłowska J.; Characterization of collagen/hydroxyapatite composite sponges as a potential bone substitute; International Journal of Biological Macromolecules, 47:483–487, 2010.

263. Sena L. A., Caraballo M. M., Rossi A.M., Soares G.A ; Synthesis and characterization of biocompomposites with different hydroxyapatite-collagen ratios ; J. Mater Sci: Mater Med, 37:2395-2400, 2009.

264. Sionkowska A., Wisniewski M., Skopinska J., Mantovani D.; Effects of solar radiation on collagen-based biomaterials; International Journal of Photoenergy ,45:1–6; 2006.

265. Al-Sagheer F., Muslim D.; Thermal and Mechanical Properties of Chitosan/$SiO_2$ Hybrid Composites; Journal of Nanomaterials, Article ID 490679, 7 pages, 2010.

303.Tomoaia Gh., L.-B. Pop, Petean I., Tomoaia-Cotisel M.; Significance of surface structure on orthopedic materials; Materiale Plastice, 49:1-12, 2012.

317. Tomoaia Gh., Soritau O., Tomoaia-Cotisel M., Pop L.-B., Pop A., Mocanu A., Horovitz O., Bobos L.-D.; The effect of self-assemblies based on nanostructured phosphates and collagen mixtures on cell cultures, in “Metal Elements in Environment, Medicine and Biology”, Editors, G. Garban and R. Silaghi-Dumitrescu, Tome IX, pp. 135-140, 2009, Cluj-Napoca University Press, ISSN: 1583-4204.

318. Tomoaia Gh., Pop L.-B., Tomoaia-Cotisel M.; Cell scaffolds mimic bone structure. The effect of calcium phosphates and collagen mixtures on osteoblasts cultures, in “Promovarea dezvoltarii durabile in spatiul Dunarean prin cooperare culturala si stiintifica”, Humboldt-Kolleg Monography, Cluj-Napoca, 20-23 May, 2010; Monography, Mediamira Press, Cluj-Napoca, pp. 233-240, 2010.

319. Tomoaia Gh., Soritau O., Tomoaia-Cotisel M., Pop L.-B., Pop A., Mocanu A., Horovitz O., Bobos L.-D.; Scaffolds made of nanostructured phosphates, collagen and chitosan for cell culture; Paper Identification P-126-Cotisel; “The 5th International Granulation Conference”, Lausanne, Switzerland, June 20-22, 2011, 18 pagini.

320. Tomoaia Gh., Tomoaia-Cotisel M., Mocanu A., Horovitz., Bobos L-D., Crisan M., Petean I.; Supramolecular organization of collagen and anti-cancer drugs; J. Optoelectronics Advanced Materials, 10:961 – 964, 2008.

321. Tomoaia Gh., Soritau O., Tomoaia-Cotisel M., Pop L.-B., Pop A., Mocanu A., Horovitz O., Bobos L.-D.; Nanostructured phosphates, collagen and chitosan scaffolds for cell culture; Journal Powder Technology, 2011, in press.

322. Prejmerean C., Tomoaia-Cotisel M., Vasile E., Furtos G., Pop L-B, Moldovan M., Sarosi C., Petean I.; Characterization of surface organization and morphology of some new experimental dental resin-based composites; International Journal of Nano and Biomaterials, 2011, in press.

323. Tomoaia Gh., Soritau O., Tomoaia-Cotisel M., Pop L.-B., Pop A., Mocanu A., Horovitz, O., Bobos L.-D.; The effect of self-assemblies based on nanostructured phosphates and collagen mixtures on cell cultures; in "The 9th International Symposium of Roumanian Academy, Cluj-Napoca Branch and Timisoara Branch", on "Metal Elements in Environment, Medicine and Biology", Cluj-Napoca, October 16-17, 2009.

324. Pop L.-B., Pop A., Tomoaia Gh., Mocanu A., Bobos L.-D., Horovitz O., Jumate N., Bratu I., Tomoaia-Cotisel M.; Synthesis and physico-chemical characterization of Inorganic powders of nano- and micro-structures based on calcium phosphates; in "The 9th International Symposium of Roumanian Academy, Cluj-Napoca Branch and Timisoara Branch", on "Metal Elements in Environment, Medicine and Biology", Cluj-Napoca, October 16-17, 2009.

325. Tomoaia Gh., Pop L.-B. , Tomoaia-Cotisel M., Cell scaffolds mimic bone structure. The effect of calcium phosphates and collagen mixtures on osteoblasts cultures, "Humboldt-Kolleg Conference", Cluj-Napoca, May 20-23, 2010.

326. Tomoaia Gh., Soritau O., Tomoaia-Cotisel M., Pop L.-B., Pop A., Mocanu A., Horovitz O., Bobos L.-D.; Scaffolds made of nanostructured phosphates, collagen and chitosan for cell cultures; "International Physical Chemistry Conference", (ROMPHYSCHEM 14, 2010), Bucharest, June 2-4, 2010.

327. Furtos G., Tomoaia-Cotisel M., Prejmerean C., Baldea B., Pop L.B., Pop A., Moldovan M.; New antimicrobial bone cement based on hydroxyapatite and silver; The 4th International Conference "Biomaterials, Tissue Engineering & Medical Devices", BiomMedD'2010, Sinaia, 23-25 September, 2010.

328. Prejmerean C., Tomoaia-Cotisel M., Furtos G., Pop L-.B., Trif M., Sarosi C., Petean I.; Characterization of surface organization and morphology of some new experimental dental resin-based composites; The 4th International Conference "Biomaterials, Tissue Engineering & Medical Devices". (Poster: P89), Sinaia, 23-25 September, 2010.

329. Tomoaia Gh., Soritau O., Pop L.-B., Furtos G., Prejmerean C., Mocanu A., Tomoaia-Cotisel M.; Scaffolds of hydroxyapatite, collagen and chitosan for improved adhesion and bioactivity of osteoblastic cells; COST Meeting, Action TD0906, University of Mons, Mons, Belgium, May 18-20, 2011.

330. Furtos G., Tomoaia-Cotisel M., Baldea B., Pop L.-B., Jumate N., Prejmerean C., Barbu T.L.; The effect of $CaF_2$ content on mechanical properties of some bone cements based on hydroxyapatite; The annual meeting of the European Chapter of the Tissue Engineering and Regenerative Medicine International Society (TERMIS), in Granada Congress and Exhibition Centre, Spain, June 7-10, 2011.

331. Tomoaia Gh., Soritau O., Tomoaia-Cotisel M., Pop L.B., Pop A., Mocanu A., Horovitz O., Bobos D.L.; The effect of self-assembled composites based on calcium phosphates and biopolymers on the adhesion of osteoblast cells; The 10$^{th}$ International Conference on Colloid and Surface Chemistry (Cea de a 10-a Conferinta de Chimia Coloizilor si a Suprafetelor cu Participare Internationala , Ediție omagială dedicată Anului Internațional al CHIMIEI – 2011), “Dunarea de jos” University of Galati, Galati, June 9-11, 2011.